https://doi.org/10.5194/egusphere-2026-1654
Preprint. Discussion started: 2 April 2026

The humidity paradox: how drier conditions and fewer clouds amplify terrestrial warming due to global climate change

Paul Glantz[1,2], Kevin J. Noone[1,2], Abhay Devasthale[3] and Frederik Schenk[2,4,5]

[1]Department of Environmental Science, Stockholm University, Stockholm, Sweden
[2]Bolin Centre for Climate Research, Stockholm University, Stockholm, Sweden
[3]Meteorological research unit. Swedish Meteorological and Hydrological Institute (SMHI), Norrköping, Sweden
[4]Department of Geological Sciences, Stockholm University, Stockholm, Sweden
[5]Department of Geosciences and Geography, University of Helsinki, Helsinki, Finland

Correspondence to: Paul Glantz (paul.glantz@aces.su.se)

Abstract. Clouds are a controlling factor determining the planetary albedo and thus strongly contribute to establishing the radiation balance at the top of the atmosphere as well as the energy balance at the surface. Terrestrial warming rates, divergent to oceans, have accelerated substantially since around 1980, along with significant changes in humidity and cloud cover. We analyse spatiotemporal changes in warming rates compared to changes in Earth's radiation and humidity, considering land globally for the period 1979–2023, using reanalysis and satellite data. We find statistically significant increases in top of the atmosphere net solar radiation and surface net terrestrial radiation, causing a net warming, together with decreasing cloud cover. These changes coincide with drier land surface conditions and are associated with the humidity paradox: insufficient supply of water vapour causing a decrease in relative humidity. Reduced evaporative cooling of the land surface is an additional positive feedback and has likely contributed to the ocean-land warming contrast. The oceans have, on the other hand, effectively unlimited water to evaporate and can therefore cool in a warming climate by evaporating more and more water. Inhibited cloud formation over land and an increase in solar radiation provide an amplifying feedback loop for the observed rapid terrestrial warming in recent decades due to a CO_2-driven humidity deficit. A decrease in precipitation over land regionally is a strong indication of perturbed surface water balance that is driven by increases in absorbed infrared and solar radiation.

1 Introduction

The Earth's climate system is highly perturbed by anthropogenic activities (IPCC, 2021), with global surface mean temperature being 1.09°C (0.95–1.20°C) higher in 2011–2020 than in 1850–1900. Evidence of a significant acceleration of global warming since 2015, after removing estimate of the influence of three natural variability factors and excluding outlier years in 2023 and 2024, is presented in the study by Foster and Rahmstorf (2026). The warming is however substantially larger over land (1.59°C [1.34–1.83] °C) than over the oceans (0.88°C [0.68–1.01] °C) and the difference has substantially increased since around 1980

https://doi.org/10.5194/egusphere-2026-1654
Preprint. Discussion started: 2 April 2026

(Figure 2.11c in Chapter 2.3.1.1.2 in IPCC, 2021). The overall global warming is mainly due to an enhanced greenhouse effect, with more infrared radiation trapped by anthropogenic greenhouse gases (IPCC, 2014, 2021). The specific heat capacity is fairly insensitive to the presence of increasing radiative forcing and can therefore not explain amplified land warming relative to ocean in a changing climate (Manabe et al., 1991; Sutton et al., 2007). An increase in globally integrated ocean heat content of the layer 0–2000m (Ishii et al., 2017) has however contributed to an increase in the ratio between land and ocean warming. About 93% of the extra heat at present has ended up as increased ocean heat content (Trenberth and Cheng, 2024). Wong and Minnett (2018) hypothesize that changes in the temperature gradient within the thermal skin layer, which is a direct effect of enhanced absorption of infrared radiation, modulate the amount of heat loss from the air-sea surface. Their analysis provides an explanation for the indirect increases in the ocean heat content through retention of heat from the absorption of solar radiation within the bulk of the ocean. The warming contrast is as well confirmed by the lapse rate (Sherwood et al., 2020; Brogli et al., 2021): land experiences a greater decrease in lapse rate, meaning less temperature decrease with height, than ocean. Moist air over the oceans has a higher heat capacity and resists changes in temperature more than dryer air over land. As the climate warms, a weaker decrease in lapse rate over land implies a larger increase in land surface temperature relative to the ocean.

While the radiative forcing by GHGs is global, long-term and short-term warming trends differ in space and time and may also vary depending on the season. In addition to internal variability, regional changes are forced by more heterogeneous perturbations, such as anthropogenic aerosols that temporarily mask greenhouse warming (Glantz et al., 2022; IPCC, 2021; Quaas et al., 2022). Europe has warmed at a rate of +0.5°C per decade since 1980s, more than twice the global average, making it the fastest warming of the continents (WMO, 2022). This is also the region where anthropogenic aerosol's largest negative mean radiative forcing reduction occurred during the last four decades (Glantz et al., 2022; IPCC, 2021). Robust evidence for a decreasing trend in aerosol climate forcing was also found globally between 2000 and 2019, and it is associated with high-quality satellite retrievals (Quaas et al., 2022). Furthermore, every month since June 2023 to so far August 2024 was the warmest globally in the European Centre for Medium-range Weather Forecasts (ECMWF) ERA5 data record, going back to 1940 (Copernicus, 2023). September 2023 exhibited the largest temperature anomaly among these months, +0.93°C above the 1991–2020 average, while June 2024 is the warmest measured since 1850. The global annual mean temperature in 2023 is 1.48 °C higher than the reference period 1850–1900. The magnitude of the warming jump in 2023 was unexpected and exceeded levels seen in previous El Niño years, with models currently being unable to explain the warming (Schmidt 2024).. Based on reliable simulations from three well-established climate model ensembles of both climate variability, such as El Niño-Southern Oscillation, and the forced response to GHG forcing, Rantanen & Laaksonen (2024) found that internal climate variability alone is unlikely to explain the unusually rapid warming that occurred in September 2023. Considering regional changes and other time frames, previous studies have nevertheless found changes in atmospheric circulation relevant for warming trends (Blanc et al., 2022; Rudeva et al., 2023; Sfică et al., 2020; Simmons, 2022).

https://doi.org/10.5194/egusphere-2026-1654
Preprint. Discussion started: 2 April 2026

While the oceans on Earth contain an essentially inexhaustible supply of water to be evaporated this does not hold for land, while a large amount is recycled (Wang et al., 2023; Trenberth et al., 2007). The moist air is advected through atmospheric circulation, and some amount is removed as precipitation over land. In the study by Wang et al. (2023) a significant increase in annual net water inflow from ocean to land of 1.48×10^{15} kg yr^{-1} $decade^{-1}$ was found with respect to the period 1980 – 2018. Based on observations and Atmospheric Model Intercomparison Project 5 (AMIP5) simulations, the air could generally take up about 7% more moisture for a temperature rise of 1 °C in the lower atmosphere when averaged globally, in line with the Clausius-Clapeyron equation (Allan et al., 2014, 2020). This is close to the finding by Wan et al. (2023), who find a somewhat higher rate of 9.5% per 1 °C globally over the period 1993–2021, based on reanalysis datasets. Even so, changes in relative humidity over the oceans under a warming climate, based on theoretical and model-based analysis, are considered insignificant or slightly positive (Byrne & O'Gorman, 2013, 2016, 2018; Douville et al., 2022; Held & Soden, 2006; Schneider, 2010).

The slower warming of the oceans at present implies, however, an expected limitation in evaporated moisture to keep pace with the rapid increase in the temperature over land (Byrne and O'Gorman, 2018; Simmons et al., 2010; Willet et al., 2024). The relative humidity over land has consequently decreased (Willet et al., 2014, 2024), which makes it harder to condense water and form clouds (Simmons et al., 2010; Willet et al., 2014, 2020) and hence increases the risk for drier periods. CMIP5 (Coupled Model Intercomparison Project Phase 5) simulations, however, underestimate this decline in relative humidity observed over land globally (Douville & Plazzotta, 2017; Dunn et al., 2017). In addition, the observational record is consistent with our physical understanding that global mean evaporation and precipitation increase more slowly (2-3%/°C), constrained by the surface energy balance, than the theoretical increase in water vapour content (7%/°C) (Allan et al., 2020). This increases the lifetime of water vapour in the atmosphere (Allan et al., 2020; Bosilovich et al, 2005; Douville et al., 2002; Schneider et al., 2010). Latent heat released through precipitation is balanced by the net atmospheric longwave radiative cooling minus the heating from absorbed sunlight and sensible heat flux from the surface. The water vapor distribution will continue to be affected as long as anthropogenic greenhouse gas concentrations increase. However, the positive feedback on the greenhouse effect is weak for water vapour in the boundary layer since the temperature is similar to the ground (Held and Soden, 2000; IPCC, 2001). In addition, half of the atmospheric water vapour is found below 850 hPa. Model simulations of the Earth's climate nevertheless indicate increases in the sensitivity of surface temperatures to carbon dioxide water vapour feedback by nearly a factor of two (Held and Soden, 2000).

Clouds affect outgoing longwave radiation in the same way as GHGs, but the net effect on the radiation budget also depends on the reflection of incoming solar radiation. As clouds form, latent heat is released due to condensation. However, the representation of clouds in global climate models (GCMs) is one of the largest sources of uncertainty in estimates of climate sensitivity (Boucher et al., 2013; Dufresne & Bony, 2008; Schneider et al., 2017; Soden and Held, 2006; Vial & Bony, 2013; Zelinka et al., 2017), mainly due to uncertainties in aerosol-cloud interactions (IPCC, 2021). Even so, cloud changes can be

https://doi.org/10.5194/egusphere-2026-1654
Preprint. Discussion started: 2 April 2026

related to more reliable estimates of changes in incoming solar radiation, based on observations carried out from space and ground.

Strong decreases in ERA5 cloud cover over large parts of Europe in the summer half year, April – September, during the last four decades are in line with increases in surface downward solar radiation from reanalysis data and ground-based measurements (Glantz et al., 2022). At the same time, drier surface conditions were found in southern Europe and France, where sensible heat flux increased at the expense of latent heat flux. The latter finding and the consequence of faster warming over land than over the oceans support a negative trend in relative humidity. Zhuang et al. (2024) concluded based on both observations and climate model simulations that drought events in the western United States, due to global warming, are mainly caused by an increase in evaporative demand and less from precipitation deficit since around 2000. Furthermore, based on independent satellite and in-situ observations, a statistically indistinguishable decadal increase in Earth's global energy imbalance of 0.50 ± 0.47 W m^{-2} per decade from mid-2005 to mid-2019 was found by Loeb et al. (2021). The authors conclude that this is primarily due to decreased reflection by clouds and sea ice as well as a decrease in outgoing longwave radiation due to increases in trace gases and water vapor. At a global scale and for clear-sky conditions, the aerosol contribution was small compared to other factors.

Based on empirical orthogonal function analysis of 42 years of reanalysis data, Liu et al. (2023) found that a reduction in near-surface relative humidity, among other meteorological variables included in the investigation, explained decreases in cloud cover over most continents. The authors suggest potential stress on the terrestrial water cycle and changes in the energy partitioning between land and ocean, all associated with global warming. Luo et al. (2024a) found that cloud cover on global scale, particularly low-level cloudiness, exhibits diurnally asymmetric trends in a warming climate. This means that cloud fraction on average decreases more during the day than at night. The results from climate model simulations indicate that the diurnally asymmetric trend is mainly driven by a trend in the lower tropospheric stability, largely caused by the increasing greenhouse gases rather than natural variability. This asymmetry, found by Luo et al. (2024a), amplifies surface warming, decreasing the daytime cloud shortwave albedo effect and increasing the night-time longwave greenhouse effect by clouds.

Based on NASA GRACE/GRACE-FO data, Chandanpurkar et al. (2025) found that the continents have been affected by unprecedented loss in terrestrial water storage since 2002, which means shrinking freshwater availability. Based on an ensemble of high-resolution global drought datasets for 1981–2022, Gebrechorkos et al. (2025) found as well that global drought severity has intensified. The areas in drought have expanded by 74% on average during the last 5 years compared with 1981–2017, where atmospheric evaporative demand contributed to 58% of this increase. Furthermore, Fang et al. (2022) investigated vapour pressure deficit, a determinant for atmospheric demand for water vapour, based on in-situ observations and reanalysis from ERA5 and Modern-Era Retrospective analysis for Research and Applications, Version 2 (MERRA2) of the period 1981–2020. They found that vapour pressure deficit increased in all climatic zones, with the strongest increase in

https://doi.org/10.5194/egusphere-2026-1654
Preprint. Discussion started: 2 April 2026

the arid zone, followed by tropical, temperate, cold and polar zones. Manabe (2019) explains why soil moisture decreases in relatively arid regions on Earth due to climate change. The increases in downward terrestrial radiation increase the total radiative energy that is potentially available for evaporation. The change in precipitation is usually small in these regions due to the export of water vapour to lower and higher latitudes. To maintain the water balance of the land surface, the actual evaporation has to be reduced in relation to potential evaporation. The latter is a measure of the atmospheric demand for water, thus the upper limit of water loss. When soil gets drier, due to limitations in precipitation, the ratio of actual evaporation to potential evaporation decreases. This also means that the fraction of radiative energy used for evaporation is reduced while sensible heat flux increases.

The present study aims to investigate potential positive feedbacks over land globally by investigating changes in surface and air humidity, clouds, solar radiation, and precipitation from ECMWF ERA5 reanalysis to accelerated ocean-land warming contrast since 1979. Impacts from changes in the solar radiation at the top of the atmosphere (TOA) on surface energy balance and air temperature have been investigated. Uncertainties in the energy balance have been investigated as well. Changes in surface heat fluxes, reflected by the Bowen ratio, give an indication of possible stress on the terrestrial water cycle. As contrasting regional extremes, we evaluate South America vs. land areas in mid- and high latitudes in the Northern Hemisphere (43°N–90°N, 180°W–180°E) during the period 1979−2023. The latter strives to investigate possible regional differences in humidity supply and cooling in infrared, relevant for the warming trend. Possible changes in land albedo for the areas in the Northern Hemisphere have also been investigated. Outcomes of water vapour response to surface air temperature over land globally, relevant for possible changes in the clouds, will be presented. Changes in precipitation during the investigation period are a fingerprint of perturbed surface water balance. To support the present findings, new studies relevant to the rapid warming that occurs over land globally have been included as well.

We first introduce the various datasets and methods in Sect. 2. In Sect. 3 we present results of ERA5 TOA radiation quantities compared to Clouds and the Earth's Radiant Energy System (CERES) and CLARA-A3 satellite radiation observations of the period 2001–2023, while also considering 1982–2023 for the latter platform. ERA5 specific humidity and relative humidity are compared to Integrated Surface Database Humidity (HadISDH) gridded humidity in-situ observations since 1979. Results of total precipitation over land globally from ERA5 compared to Global Precipitation Climatology Project (GPCP) and Global Precipitation Climatology Centre (GPCC) are presented in Sect. 3. Section 4 provides a discussion of changes in radiation, humidity, cloud cover, and precipitation driven by the anthropogenic reinforced greenhouse effect and ocean-land warming contrast. Conclusions are presented in Section 5.

https://doi.org/10.5194/egusphere-2026-1654
Preprint. Discussion started: 2 April 2026

2 Data and Methods

The generation of consistent atmospheric datasets remains challenging, requiring a good knowledge of their creation and potential limitations. Hence, we combine our analysis of changes in various quantities with a comparison across different datasets to identify potential product-specific anomalies that may distort the evaluation of changes in the climate system. We briefly describe the specifics of these datasets below.

2.1 ERA5 meteorological reanalysis

ERA5 is the fifth-generation reanalysis from ECMWF, described in Hersbach et al. (2020), that combines model data with historical satellite and in situ measurements into a globally complete and consistent data set. ERA5 provides substantially improved horizontal resolution of 31 km from 1940, compared to 80 km for the previous ERA-Interim version. In the study by Johannsen et al. (2020), reduced biases in ERA5 temperatures compared to older versions of the reanalysis was found. ERA5 radiation, heat flux, temperature, humidity and precipitation data from 1979 are used in the present study. The previous period, 1940–1978, is based on a sparser observation system; for example, no satellite data before 1970 are included in the reanalysis. In the ERA5 reanalysis meteorological parameters (temperature, pressure, wind, and humidity) are pushed toward observations every few hours using data assimilation. The effect of aerosols on radiative transfer, from the study by Tegan et al. (1997), is based on prescribed climatological distributions of optical thickness from sea salt, soil/dust, organic, black carbon, and sulphate . The CMIP5 data set, derived from observations, is used in ERA5 for long-term aerosol trends (Hersbach et al., 2015). ERA5 assimilates humidity measurements from in-situ stations, radiosondes, dropsondes, and aircraft, as well as radiance measurements that are sensitive to humidity and temperature. Estimates of near-surface soil moisture from scattermeter are also assimilated into ERA5. However, discrepancies in ERA5 humidity over tropical oceans before the mid-1990s are found compared to microwave-sounding estimates, but it compares well over tropical land (Allan et al., 2022). The radiation calculations in ERA5 use thus diagnostic fields of temperature, pressure, water vapor, aerosols, and cloud properties, some of which are less constrained by observations than others and therefore induce uncertainties. The energy imbalance at the surface in ERA5 is suggested to be in the order of 4 W m^{-2} (Hersbach et al., 2020). Land and ocean pixels are identified as grid boxes with values of the ERA5 land sea mask, in the range 0 – 1, higher and lower than 0.5, respectively.

2.2 CERES satellite radiation observations

CERES Energy Balanced Filled (EBAF) TOA Edition 4.2 data product (Doelling et al., 2013, 2016; Loeb et al., 2018), mounted on the Terra and Aqua spacecraft launched in 1999 and 2002, respectively, has been used in our analysis. The mean local time for descending across the equator is around 10:30 for Terra, while *Aqua* ascends across the equator around 13:30 mean local time. Terra carries the CERES FM1 and FM2 instruments and Aqua carries the CERES FM3 and FM4 instruments. Each instrument measures filtered broadband radiances in shortwave (SW; 0.3–5.0 μm) and longwave window channels (8.0–12.0 μm). Total radiation solar and terrestrial radiation (0.3-200 µm) – is measured as well. Longwave radiances are obtained

https://doi.org/10.5194/egusphere-2026-1654
Preprint. Discussion started: 2 April 2026

from total minus SW radiations. The CERES project combines Terra and Aqua Moderate Resolution Imaging Spectroradiometer (MODIS) and geostationary satellite observations, snow cover and sea ice extent derived from microwave instruments, and thermodynamic variables from reanalysis. The aim is to improve estimates of TOA and surface irradiance. The overall uncertainty in monthly all-sky TOA flux, with respect to 1° ∗ 1° latitude-longitude area, is estimated to be 3 W m^{-2} (1σ) for Terra and 2.5 W m^{-2} for Terra and Aqua combined, for both shortwave and longwave fluxes (Loeb et a., 2018). However, a transition from the Terra and Aqua record to NOAA20-measurements from April 2022 onward has been carried out, since the orbits for Terra and Aqua drifted outside their maintained 15-minute local equator crossing time. The NOAA20's Visible Infrared Imaging Radiometer Suite (VIIRS) and Cross-track Infrared Sounder are in place of MODIS and Atmospheric Infrared Sounder (AIRS).

The algorithm to produce the CERES Edition 4.0 EBAF-surface data product forces calculated TOA solar and terrestrial radiation to match with CERES TOA measured irradiances by adjusting surface, cloud, and atmospheric properties (Kato et al., 2018). Surface downward solar radiation are accordingly adjusted with respect to a radiative kernel technique: quantifying radiative biases caused by geophysical variables. The irradiances are calculated based on temperature and specific humidity between the heights 200 and 500 hPa, and biases in these variables are corrected according to observations by AIRS. Bias in the cloud fraction is corrected in the same way, while in this case based on observations by Cloud Aerosol Lidar and Infrared Pathfinder Satellite Observations (CALIPSO) and CloudSat. The remaining errors in surface, cloud, and atmospheric properties are corrected using a Lagrange multiplier to eliminate differences that occur between calculated and observed solar and terrestrial radiation at the TOA. (Kato et al., 2013; Rose et al., 2013). In the study by Kato et al. (2018) estimations of uncertainties in all-sky global annual mean upward and surface downward solar radiation over land, ocean and polar regions are found to be 3 and 4 W m^{-2}, respectively. In addition, the uncertainties for upward and downward surface terrestrial radiation are 3 and 6 W m^{-2}, respectively.

2.3 CLARA-A3 radiation climate data record

In the present study we have investigated TOA and surface radiation products derived from the long-term Advanced Very High-Resolution Radiometer (AVHRR) sensors flown onboard NOAA and EUMETSAT MetOp satellites. These products were derived in the framework of EUMETSAT's Satellite Application Facility on Climate Monitoring CM SAF, (Schulz et al., 2009). The radiation variables, described in Karlsson et al. (2023a; 2023b), are part of a suite of cloud and radiation products provided in the third edition of CM SAF's CLoud, Albedo and surface RAdiation (CLARA-A3) dataset from AVHRR. CLARA-A3 offers substantial improvements to its previous version, CLARA-A2 (Karlsson et al., 2017), and recent studies show that the product is one of the most stable cloud climate data records (Devasthale and Karlsson, 2023; Devasthale et al., 2025). We specifically used here the Level 3 monthly means of radiation products that are available at a 0.25-degree spatial resolution globally from 1982 through 2023. Land and ocean pixels are identified as grid boxes with values of the CLARA-A3 land sea mask, in the range 0 – 100, higher and lower than 50, respectively. The drifting of NOAA satellites can

https://doi.org/10.5194/egusphere-2026-1654
Preprint. Discussion started: 2 April 2026

induce artificial trends in the time-series of the retrieved parameters (Devasthale et al., 2012; Bojanowski and Musial, 2020). To mitigate this, we use the AVPOS version of CLARA-A3 that are based on all available satellites and we draw conclusions based on the analysis of other independent datasets as well. We do however take extra care in interpreting the trends in the CLARA-A3 after 2020 when the drift signal could be stronger.

2.4 HadISDH humidity in-situ land observations

HadISDH is a global gridded monthly mean *in-situ* land surface humidity dataset (version: 4.6.0.2023f) based on a quality-controlled sub-daily dataset described in more detailed in Smith et al. (2011a) and Willet et al. (2014). This dataset relies on an integrated surface database from the National Oceanic and Atmospheric Administration's (NOAA's) National Centers for Environmental Information (NCEI) with hourly measured dew point temperature and air temperature converted to various humidity variables. These variables are homogenized and averaged over a period of one month over 5° by 5° grid boxes. The hourly station data passes through several stages of processing before being gridded. The quality-controlled hourly temperatures are converted to specific and relative humidity, based on relevant equations, at each time point. For relative humidity, dry biases could be up to 4%, which increases with wet bulb temperature toward 0°C. The potential error of specific humidity for temperature differences (from climatology) of ±20 °C is estimated to be 1% of the individual hourly values obtained from the majority, 89%, of the in-situ stations. These sites are located below 1000 m. The data coverage from HadISDH is very poor in the Southern Hemisphere, while also at some regions in the Northern Hemisphere.

2.5 GPCP total annual precipitation amount

The GPCP Version 3.3 provides analyses of monthly precipitation on a 0.5° × 0.5° latitude–longitude global grid for the period from 1983 to 2023. This merged product continues the GPCP heritage of incorporating precipitation estimates from low-orbit satellite microwave data, geosynchronous-orbit satellite infrared data, sounder-based estimates, and surface rain gauge observations. The aim is to emphasize the strengths of various inputs and strive for temporal and spatial homogeneity. The analysis incorporates modern algorithms, refined intercalibrations among sensors, climatologies of recent high-quality satellite precipitation data, and fine-scale multi-satellite estimates. New data fields have been introduced to better characterize precipitation, including the fraction of the precipitation that is liquid (rain). Homogeneity in the record takes precedence over instantaneous accuracy. Over the long-term, GPCP represents the current state of the art. GPCP estimates are most accurate in the tropics and less so in the subtropics and mid-latitudes. Above 58° north and below 58° south, the estimates are more approximate. High-quality GPCC gauge analyses are incorporated to vastly improve the estimates over land. For more information about the GPCP Version 3 data, see Huffman et al. (2023).

2.6 GPCC total annual precipitation amount

The GPCC Full Data Monthly Product Version 2025, based on gauge observations that cover the period from 1983 to 2023 has been investigated in the present study. This new product was generated in November 2025 and uses the new GPCC

https://doi.org/10.5194/egusphere-2026-1654
Preprint. Discussion started: 2 April 2026

climatology as an analysis background. The analysis product is based on all ground-based stations, near real-time and non-real-time, in the GPCC database. The data coverage per month varies from less than 10,000 to more than 52,000 stations. Precipitation anomalies at the stations are interpolated and then superimposed on the GPCC Climatology V2025. This product contains monthly totals on a regular grid with the spatial resolution of 0.5° x 0.5° latitude by longitude used in the present study. The Full Data Monthly Product will be updated at irregular time intervals after significant database improvements. For more information about the global land-surface precipitation data product from GPCC, see Becker et al. (2013) and Schneider et al. (2014).

2.7 Statistical analysis

Global land annual mean values of the parameters from ERA5, CERES, and CLARA-A3 grid fields have been area-weighted before the analyses, with the exception of the HadISDH dataset, due to low spatial coverage. The following equations are used:

$$\mu_w = \frac{\sum_{i=1}^{N} w_i y_i}{\sum_{i=1}^{N} w_i} \quad (1)$$

$$S_w = \sqrt{\frac{\sum_{i=1}^{N} w_i \, |y_i - \mu_w|^2}{\sum_{i=1}^{N} w_i}} \quad (2)$$

where μ_w is the area-weighted mean, w_i is the area weight, y_i represent reanalysis and satellite data and S_w is the area-weighted standard deviation.

The Mann-Kendall test was used (Kendall, 1975) to investigate parameter trends according to the producer's available data records. This non-parametric technique tests for a monotonic trend in a time series and is not dependent on the distribution of the data. The null hypothesis of trend absence in the ERA5 and CERES data has been tested against the alternate hypothesis of a trend. In addition, the Wilcoxon signed-rank test (Wilcoxon, 1945) was used to test the null hypothesis that data of surface radiation budgets belonging to South America and areas in the Northern Hemisphere with different lengths have equal means, against the alternative that they don´t.

The following statistical indicators are used in our analysis:

$$\mathrm{RMSD} = \left[\frac{1}{n}\sum_{i=1}^{n}(y_i - x_i)^2\right]^{\frac{1}{2}} \quad (3)$$

$$\mathrm{NRMSD} = \frac{RMSD}{meanX} \quad (4)$$

$$R^2 = 1 - \frac{SS_{res}}{SS_{tot}} \quad (5)$$

$$\mathrm{MBE} = \frac{1}{n}\sum_{i=1}^{n}(y_i - x_i) \quad (6)$$

https://doi.org/10.5194/egusphere-2026-1654
Preprint. Discussion started: 2 April 2026

where RMSD is the root mean square deviation, NRMSD is the normalized RMSD, R^2 is the coefficient of determination, SS_{res} and SS_{tot} are the residual sum of squares and total sum of squares, respectively, and MBE is the mean bias error, y_i and x_i represent ERA5 and CERES data, respectively, meanX is mean x_i.

3 Results

3.1 ERA5 compared to CERES and CLARA-A3 time series since 2001

Figure 1 shows trends in ERA5 and CERES annual surface skin temperature, TOA net solar and upward terrestrial radiation, and surface net terrestrial radiation, obtained by linear regression during the period 2001–2023. Increases over land globally,

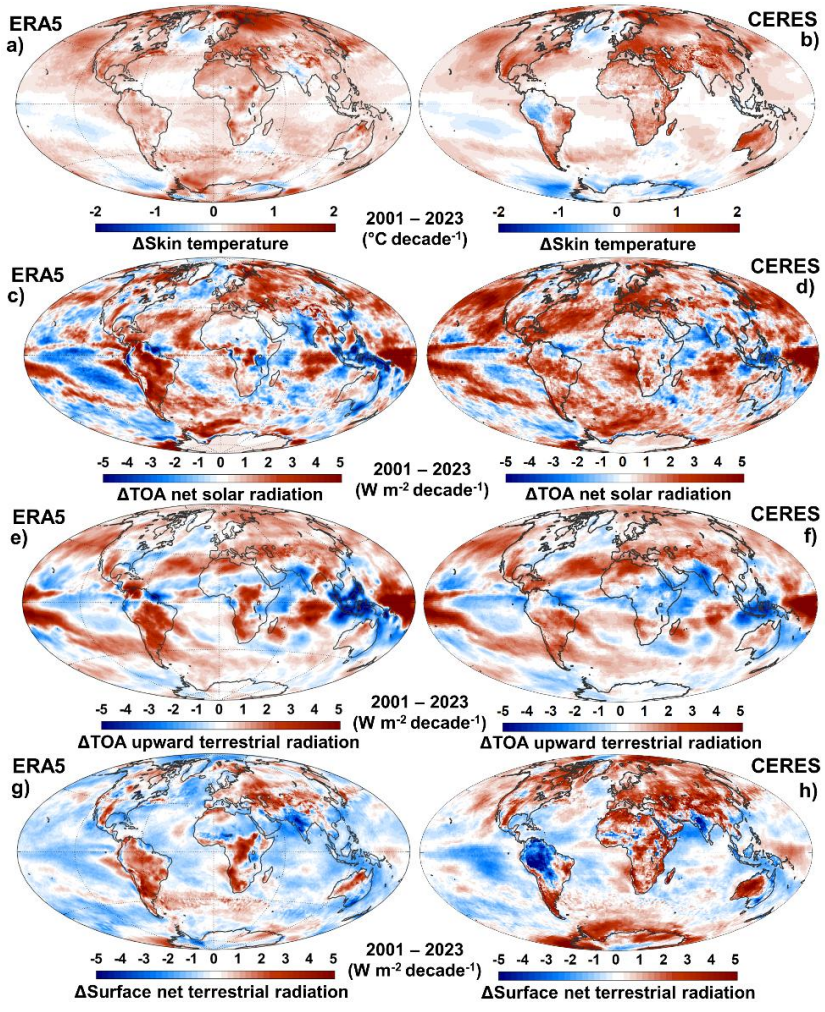

Figure 1. Comparison of annual trends in ERA5 and CERES surface skin temperature in a) and b), top of the atmosphere (TOA) net solar radiation in c) and d), TOA upward terrestrial radiation in e) and f) and surface net terrestrial radiation in g) and h), respectively. All trends were obtained by linear regression of the period 2001–2023.

https://doi.org/10.5194/egusphere-2026-1654
Preprint. Discussion started: 2 April 2026

shown in the figures, are statistically significant at the 95% confidence level, with the exception for CERES TOA upward terrestrial radiation (Table 1). A different sign of the trend in skin temperature shown in Fig. 1a and 1b appears between ERA5 and CERES over the large northern part of South America. It explains the substantially weaker increase in CERES mean skin temperature for the continent (Table 1). The increase in ERA5 temperature at two metres height is 0.23 ±0.15 °C per decade of the period 2001¬2023 for South America and as for the ERA5 skin temperature a varying degree of positive trends are found across the continent (not shown). Thus, the negative trends in CERES skin temperature over the northern part of South America do not appear in ERA5 surface air temperature. Furthermore, both ERA5 and CERES give negative trends in TOA net solar radiation and upward terrestrial radiation over South Asia, shown in Fig. 1, simultaneously as weak changes or even decreases in skin temperature appear in the same region.

A summary of comparisons between ERA5 and CERES monthly values for land globally is presented in Table 1. The range in normalized root mean square deviation (NRMSD) for ERA5 and CERES is 0.6–17%. The table shows reasonable agreements in positive trends between the datasets. However, a large deviation is found for surface net terrestrial radiation, reflected by the highest NRMSD value, where ERA5 gives the weakest increase that is not statistically significant. Table 1 shows, however, better agreement between ERA5 and CLARA-A3 surface net terrestrial radiation, considering comparisons of both global monthly mean values and annual trends. Substantially stronger trends in ERA5 TOA net terrestrial radiation than for CERES appear for land globally and South America. Stronger trends are found as well for CLARA-A3, in line with ERA5, with respect to the longer period in Fig. 2f and Table 2.

Table 1 shows low NRSMD values in the comparison between ERA5 and CERES for South America and the areas in the Northern Hemisphere of the period 2001–2023, except for surface net terrestrial radiation, where very large differences appear. Reasonable agreements are found in positive trends for these regions, with the exception for surface net terrestrial radiation. Even larger deviations are thus found regionally for this quantity, and the trend is surprisingly even of the opposite sign for South America. This explains the weaker increase in the CERES skin temperature compared to ERA5. In addition to land globally, Table 1 shows substantially better agreements in surface net terrestrial radiation between ERA5 and CLARA-A3 when considering both these regions. The trends agree also much better between these data sources. The changes over the two regions investigated are statistically significant at the 95% confidence level for all the ERA5 and CLARA-A3 cases, while not for CERES skin temperature and TOA upward terrestrial radiation in South America (Table 1).

https://doi.org/10.5194/egusphere-2026-1654
Preprint. Discussion started: 2 April 2026

Table 1. Comparisons between ERA5 and CERES monthly area-weighted mean (< >) skin temperature (T_{skin}), TOA net solar radiation and upward terrestrial radiation (SR and TR, respectively), and surface net SR and TR. Annual trends (Δ) with 95% confidence bounds of the period 2001 – 2023 over land globally are presented. Results of CLARA-A3 surface net TR of the are also shown.

Land globally								
Parameter	**R^2**	**RMSD[a]**	**NRMSD[b]**	**MBE[c]**	**<ERA5>**	**<CERES>**	**ΔERA5**	**ΔCERES**
$T_{skin}^{E,C}$	1	2.0 (°C)	17.4 (%)	-1.7 (°C)	9.6 ±4.5 (°C)	11.3 ±3.6 (°C)	0.36 (0.25, 0.47) (°C decade^{-1})	0.33 (0.21, 0.44) (°C decade^{-1})
TOA net $SR^{E,C}$	1	8.0 (W m^{-2})	3.6 (%)	-6.7 (W m^{-2})	215.0 ±31.7 (W m^{-2})	221.8 ±27.5 (W m^{-2})	0.57 (0.25, 0.88) (W m^{-2} decade^{-1})	0.67 (0.37, 0.97) (W m^{-2} decade^{-1})
TOAupward TR^{E}	1	1.29 (W m^{-2})	0.55 (%)	-0.25 (W m^{-2})	233.6 ±8.3 (W m^{-2})	233.8±7.2 (W m^{-2})	0.50 (0.18, 0.83) (W m^{-2} decade^{-1})	0.26 (-0.10, 0.63) (W m^{-2} decade^{-1})
Surface net $SR^{E,C}$	1	8.7 (W m^{-2})	5.9 (%)	-8.4 (W m^{-2})	138.6 ±20.4 (W m^{-2})	147.0 ±18.2 (W m^{-2})	0.52 (0.16, 0.88) (W m^{-2} decade^{-1})	0.74 (0.48, 1.00) (W m^{-2} decade^{-1})
Surface net TR^{C}	0.43	8.5 (W m^{-2})	14.3 (%)	8.0 (W m^{-2})	67.5 ±3.7 (W m^{-2})	59.5 ±1.4 (W m^{-2})	0.23 (-0.04, 0.51) (W m^{-2} decade^{-1})	0.72 (0.46,0.98) (W m^{-2} decade^{-1})
Parameter	**R^2**	**RMSD[1]**	**NRMSD[2]**	**MBE[3]**	**<ERA5>**	**<CLARA>**	**ΔERA5**	**ΔCLARA-A3**
Surface net TR^{C-A3}	0.99	2.5 (W m^{-2})	3.5 (%)	-2.4 (W m^{-2})	67.5 ±3.7 (W m^{-2})	70.0 ±3.6 (W m^{-2})	0.23 (-0.04, 0.51) (W m^{-2} decade^{-1})	0.29 (0.02, 0.56) (W m^{-2} decade^{-1})
South America								
Parameter	**R^2**	**RMSD[a]**	**NRMSD[b]**	**MBE[c]**	**<ERA5>**	**<CERES>**	**ΔERA5**	**ΔCERES**
T_{skin}^{E}	0.98	1.02 (°C)	4.8 (%)	0.98 (°C)	22.2 ±1.9 (°C)	21.2±1.9 (°C)	0.28 (0.14, 0.41) (°C decade^{-1})	0.15 (-0.03, 0.34) (°C decade^{-1})
TOA net $SR^{E,C}$	0.98	6.0 (W m^{-2})	2.2 (%)	-1.4 (W m^{-2})	271.3 ±36.2 (W m^{-2})	272.7 ±37.8 (W m^{-2})	1.97 (0.92, 3.02) (W m^{-2} decade^{-1})	1.07 (0.41, 1.73) (W m^{-2} decade^{-1})
TOAupward TR^{E}	0.94	3.5 (W m^{-2})	1.4 (%)	0.83 (W m^{-2})	243.4 ±9.4 (W m^{-2})	242.6 ±6.6 (W m^{-2})	1.41 (0.32, 2.50) (W m^{-2} decade^{-1})	0.70 (-0.01, 1.49) (W m^{-2} decade^{-1})
Surface net $SR^{E,C}$	0.94	6.0 (W m^{-2})	3.3 (%)	-1.0 (W m^{-2})	178.8 ±24.4 (W m^{-2})	178.8 ±24.6 (W m^{-2})	2.29 (1.11, 3.46) (W m^{-2} decade^{-1})	2.08 (1.29, 2.88) (W m^{-2} decade^{-1})
Surface net $TR^{E,C}$		13.1 (W m^{-2})	29.6 (%)	11.7 (W m^{-2})	56.1 ±5.5 (W m^{-2})	44.4 ±2.1 (W m^{-2})	1.28 (0.63, 1.94) (W m^{-2} decade^{-1})	-1.11 (-1.39, -0.82) (W m^{-2} decade^{-1})
Parameter	**R^2**	**RMSD[a]**	**NRMSD[b]**	**MBE[c]**	**<ERA5>**	**<CLARA>**	**ΔERA5**	**ΔCLARA-A3**
Surface net $TR^{E, C-A3}$	0.99	0.97 (W m^{-2})	1.7 (%)	-0.88 (W m^{-2})	56.1 ±5.5 (W m^{-2})	56.9 ±5.4 (W m^{-2})	1.28 (0.63, 1.94) (W m^{-2} decade^{-1})	1.25 (0.62, 1.87) (W m^{-2} decade^{-1})
Northern Hemisphere part								
Parameter	**R^2**	**RMSD[a]**	**NRMSD[b]**	**MBE[c]**	**<ERA5>**	**<CERES>**	**ΔERA5**	**ΔCERES**
$T_{skin}^{E,C}$	1	2.7 (°C)	1.3 (%)	2.7 (°C)	-1.6 ±12.6 (°C)	-2.8 ±11.2 (°C)	0.52 (0.31, 0.72) (°C decade^{-1})	0.43 (0.27, 0.60) (°C decade^{-1})
TOA net $SR^{E,C}$	1	8.5 (W m^{-2})	5.8 (%)	7.7 (W m^{-2})	153.8 ±100 (W m^{-2})	146.1±100.0 (W m^{-2})	1.00 (0.61, 1.41) (W m^{-2} decade^{-1})	0.86 (0.51, 1.22) (W m^{-2} decade^{-1})
TOAupward $TR^{E,C}$	1	1.2 (W m^{-2})	0.58 (%)	-0.72 (W m^{-2})	211.1 ±21.2 (W m^{-2})	211.9 ±20.4 (W m^{-2})	0.68 (0.33, 1.02) (W m^{-2} decade^{-1})	0.55 (0.23, 0.86) (W m^{-2} decade^{-1})
Surface net $SR^{E,C}$	1	2.1 (W m^{-2})	2.3 (%)	1.4 (W m^{-2})	95.0 ±64.6 (W m^{-2})	93.7 ±65.1 (W m^{-2})	1.06 (0.63, 1.49) (W m^{-2} decade^{-1})	0.94 (0.62, 1.26) (W m^{-2} decade^{-1})
Surface net $TR^{E,C}$	0.78	10.8 (W m^{-2})	24.3 (%)	7.2 (W m^{-2})	51.8 ±11.4 (W m^{-2})	44.6 ±3.8 (W m^{-2})	0.33 (0.05, 0.62) (W m^{-2} decade^{-1})	1.22 (0.90, 1.54) (W m^{-2} decade^{-1})
Parameter	**R^2**	**RMSD[a]**	**NRMSD[b]**	**MBE[c]**	**<ERA5>**	**<CLARA>**	**ΔERA5**	**ΔCLARA-A3**
Surface net $TR^{E, C-A3}$	0.99	5.0 (W m^{-2})	8,9 (%)	-4.8 (W m^{-2})	51.8 ±11.4 (W m^{-2})	56.7 ±10.3 (W m^{-2})	0.33 (0.05, 0.62) (W m^{-2} decade^{-1})	0.42 (0.13, 0.70) (W m^{-2} decade^{-1})

[a]Root mean square deviation, [b]Normalized RMSD, [c]MBE = mean bias error, [E, C & C-A3]Statistically significant at the 95% confidence level for trends (Mann-Kendall test) for annual mean of the period 2000 - 2023 for ERA5, CERES and CLARA-A3, respectively.

https://doi.org/10.5194/egusphere-2026-1654
Preprint. Discussion started: 2 April 2026

3.2 ERA5 compared to CLARA-A3 time series since 1982

Comparisons of TOA upward solar and terrestrial radiation from ERA5 and CLARA-A3 for land globally of the longer investigation period 1982–2023 are presented in Fig. 2. There are no results presented for CLARA-A3 TOA upward solar radiation over parts of South America and Australia, shown in Fig. 2b, since several years of the data record are not complete for annual averaging. Figure 2 shows as well results of ERA5 and CLARA-A3 surface net terrestrial radiation with respect to

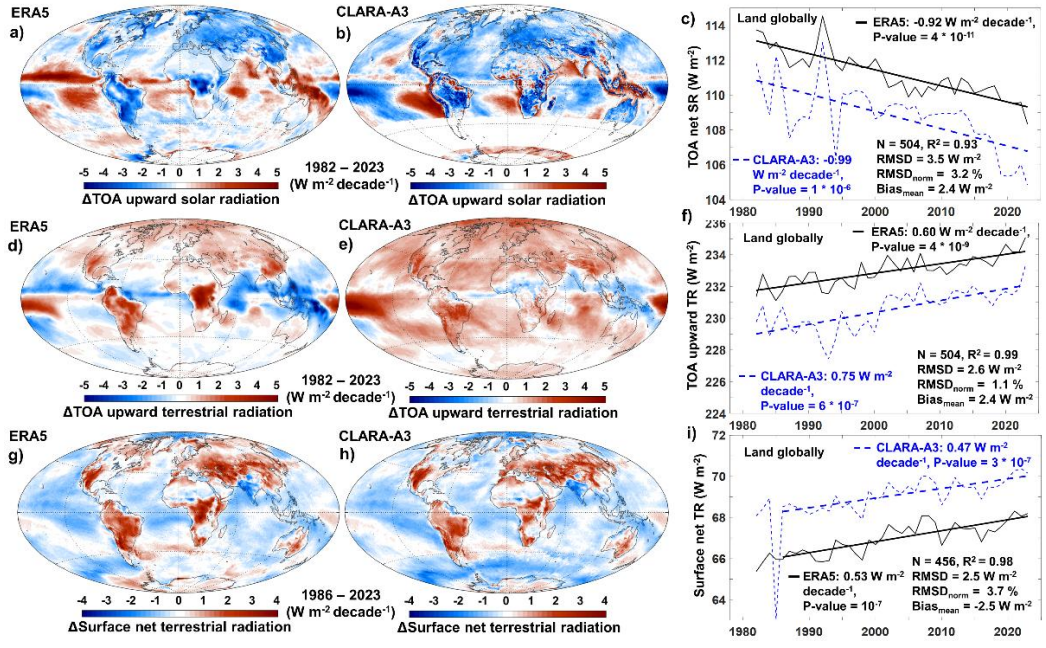

Figure 2. Annual trends in ERA5 and CLARA-A3 top of the atmosphere (TOA) upward solar radiation in a) - c), TOA upward terrestrial radiation in d) - f), and surface net terrestrial radiation in g) - i) based on linear regressions of the periods given in the figures, where p-values are obtained by Mann-Kendall test at the 95% confidence level. Heavy solid and dashed lines denote linear fits of the annual time series represented by the light solid and dashed lines. The descriptive statistics are obtained by comparing ERA5 and CLARA-A3 monthly mean values of the respective periods.

the period 1986-2023. Since CLARA-A3 is missing data globally for this quantity for February 1985, the shorter period above is included here in the estimations of trends (Fig. 2i). Good agreements between ERA5 and CLARA-A3 radiation quantities at the TOA and surface, based on monthly averaging over land globally, are found with low NRMSD values shown in Figure 2. Statistically significant negative and positive trends appear in solar and terrestrial radiation as well. ERA5 and CLARA-A3 show stronger positive trends in mean surface net terrestrial radiation over land globally since 1986 (Fig. 2i) than for the shorter investigation period 2001–2023 (Table 1). The decrease in ERA5 TOA upward terrestrial radiation is weaker compared to CLARA-A3 and large differences appears in central Africa. Regional differences in TOA upward solar radiation are also shown for Africa.

https://doi.org/10.5194/egusphere-2026-1654
Preprint. Discussion started: 2 April 2026

Table 2 shows good agreement with overall low bias between ERA5 and CLARA-A3 TOA upward solar and terrestrial radiation as well as surface net terrestrial radiation of the periods 1982–2023 and 1986–2023, respectively. This is found also in the comparisons of trends, although larger differences appear for the cases belonging to the areas in the Northern

Table 2. Comparisons between ERA5 and CLARA-A3 monthly area-weighted mean (< >) top-of-atmosphere (TOA) upward solar and terrestrial radiation (SR and TR, respectively) of the period 1982 - 2023, and surface net TR of the period 1986 - 2023 as well as [a]Root mean square deviation, [b]Normalized RMSD and [c]MBE = mean bias error. All cases are statistically significant at the 95% confidence level for annual trends according to Mann-Kendall test. TOA upward SR is calculated for South America for the areas with available values for CLARA-A3 shown in Fig. 2b.

Parameter	R^2	RMSD[a] ($W\ m^{-2}$)	NRMSD[b] (%)	MBE[c] ($W\ m^{-2}$)	<ERA5> ($W\ m^{-2}$)	<CLARA> ($W\ m^{-2}$)	ΔERA5 ($W\ m^{-2}\ decade^{-1}$)	ΔCLARA ($W\ m^{-2}\ decade^{-1}$)
South America								
TOA upward SR	0.97	8.1	6.7	7.2	128.5 ±19.9	121.3 ±20.2	-1.72 (-2.17, -1.26)	-1.64 (-2.15, -1.13)
TOA upward TR	0.96	4.1	1.7	3.6	242.2 ±9.4	238.6 ±8.7	1.26 (0.84, 1.69)	1.20 (0.79, 1.61)
Surface net TR	0.99	1.2	2.1	-1.1	55.2 ±5.2	56.3 ±5.1	1.14 (0.86, 1.42)	0.96 (0.69, 1.22)
Northern Hemisphere part								
TOA upward SR	1	2.7	2.8	0.25	97.4 ±50.7	97.2 ±49.2	-1.26 (-1.47, -1.04)	-0.98 (-1.33, -0.63)
TOA upward TR	1	2.0	0.95	1.6	210.5 ±21.1	208.9 ±21.6	0.61 (0.46, 0.76)	0.89 (0.71, 1.08)
Surface net TR	0.99	5.2	9.2	-5.0	51.4 ±11.1	56.4 ±10.4	0.54 (0.42, 0.67)	0.40 (0.26, 0.54)

[a]Root mean square deviation, [b]Normalized RMSD and [c]MBE = mean bias error. All cases are statistically significant at the 95% confidence level for annual trends according to Mann-Kendall test. TOA upward SR is calculated for South America for the areas with available values for CLARA-A3 shown in Figure 2b.

Hemisphere. Stronger decreases in reflected solar radiation and concomitant increases in absorbed energy at ground appear for South America compared to the areas in the Northern Hemisphere. Stronger increases in surface net terrestrial radiation and thus expected enhanced reduced cooling in infrared for South America are consequently found for both ERA5 and CLARA-A3.

3.3 ERA5 compared to HadISDH gridded humidity in-situ observations since 1979

Figure 3 compares ERA5 and HadISDH RH in the lower troposphere over land globally for the period 1979–2023. RMSD, NRMSD, and mean bias error between ERA5 and HadISDH monthly values are 6.3%, 9.1%, and 0.98%, respectively, based on available data from the latter data source. Figures 3a and 3b highlight deviations in mean RH for 2023 relative to the 1981–

https://doi.org/10.5194/egusphere-2026-1654
Preprint. Discussion started: 2 April 2026

2010 mean, while Fig. 3c displays the long-term trends. A stronger negative trend in ERA5 RH compared to HadiSDH shown in Fig. 3c appears as well for the case when the former data set spatially matches coverage of the in-situ data set (Willet et al., 2024). A similar and somewhat stronger negative trend than HadISDH RH is also found for JRA-3Q (developed by the Japan Meteorological Agency, Kosaka et al., 2024) over land globally for the period 1979–2023 (Willet et al., 2024). Furthermore, negative trends in relative humidity (RH) dominate over land in the Northern Hemisphere, also for HadISDH, while both data records are associated with a positive trend over parts of South Asia.

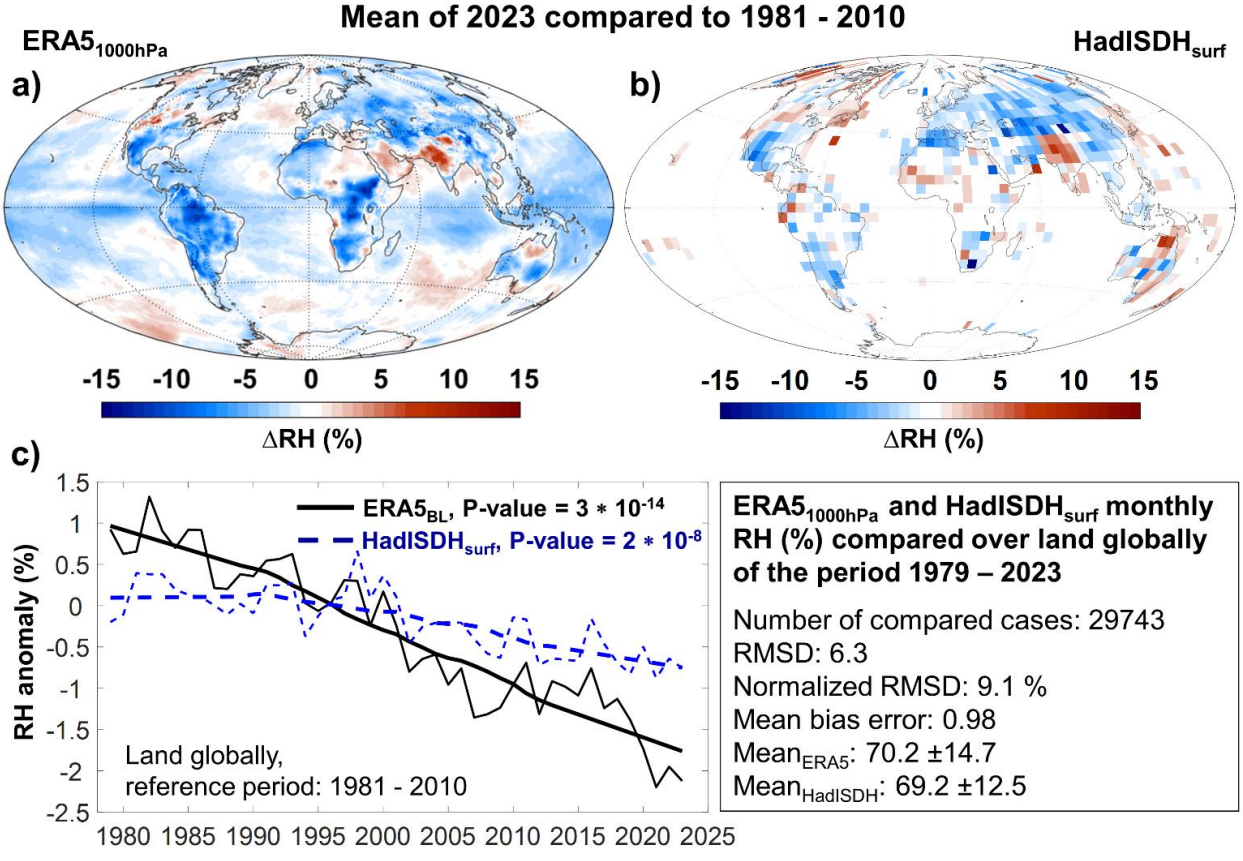

Figure 3. Comparison of relative humidity (RH) in the lower troposphere between a) ERA5 and b) HadISDH for 2023 relative to the period 1981–2010. Heavy black solid and blue dashed lines for ERA5 and HadISDH, respectively, in c) denote trend lines where the Savitzky-Golay finite impulse response smoothing filter of polynomial order has been applied on annual and global land time series represented by the light black solid and blue dashed lines. P-values of the trends are obtained by the Mann-Kendall test at the 95% confidence interval applied to the annual values. The descriptive statistics in the lower right were obtained by comparing the monthly mean values of the ERA5 and HadISDH time series.

https://doi.org/10.5194/egusphere-2026-1654
Preprint. Discussion started: 2 April 2026

Positive annual trends in specific humidity in the lower troposphere dominate in the Northern Hemisphere for both ERA5 and HadISDH, including South Asia (Fig. 4). The former data series gives trends of opposite signs in the Southern Hemisphere. These findings appear more obvious when comparing South America with the present area in the Northern Hemisphere, shown in Fig. 6f and 7f, respectively. This suggests that the HadISDH annual global trend in Fig. 4 may be overestimated due to a lack of data in the Southern Hemisphere. Good agreement appears between ERA5 and HadISDH specific humidity trends when the former data set spatially matches coverage of the in-situ data set (Willet et al., 2024).

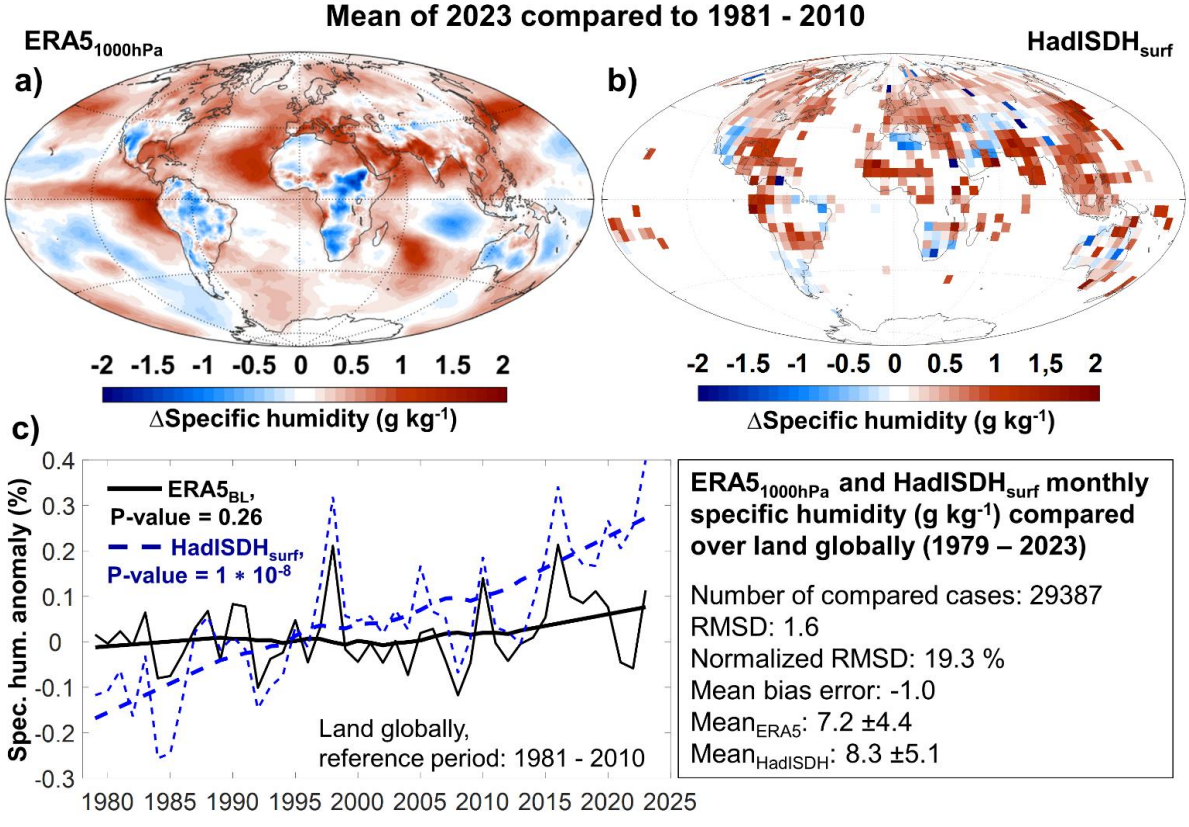

Figure 4. Comparison of specific humidity in the lower troposphere between a) ERA5 and b) HadISDH for 2023 relative to the period 1981-2010. Heavy black solid and blue dashed lines for ERA5 and HadISDH, respectively, in c) denote trend lines where the Savitzky-Golay finite impulse response smoothing filter of polynomial order has been applied on annual and global land time series represented by the light black solid and blue dashed lines. P-values of the trends are obtained by the Mann-Kendall test at the 95% confidence interval applied to the annual values. The descriptive statistics in the lower right were obtained by comparing the monthly mean values of the ERA5 and HadISDH time series.

A distinct positive trend in specific humidity during the period 1979–2024 appears as well for JRA-3Q (Willet et al., 2024). A larger deviation is found, shown in Fig. 3 and 4, in the statistics between ERA5 and HadISDH monthly specific humidity than for RH.

https://doi.org/10.5194/egusphere-2026-1654
Preprint. Discussion started: 2 April 2026

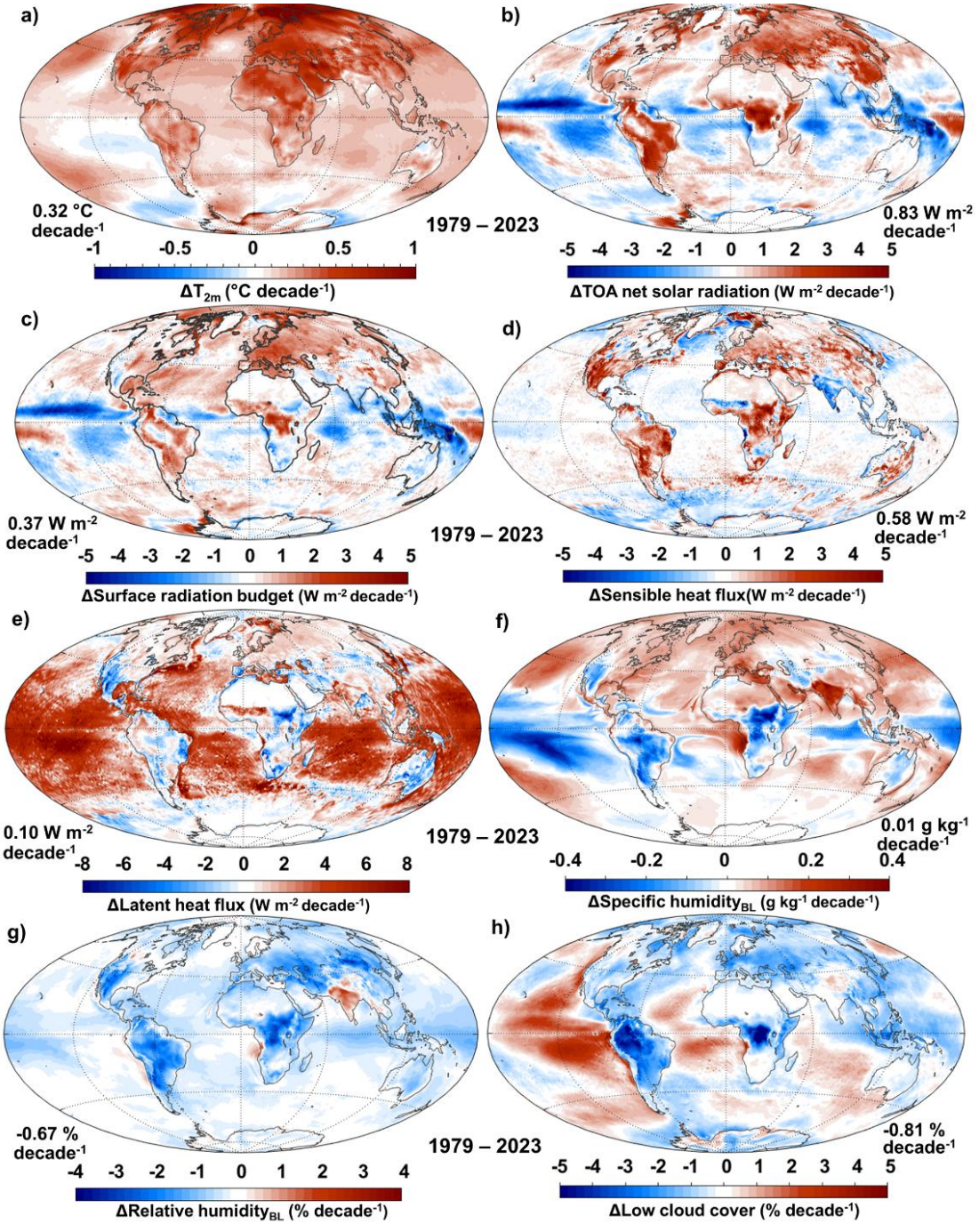

Figure 5. Trends in ERA5 a) temperature at two-metre height (T_{2m}), b) top of the atmosphere (TOA) net solar radiation, c) surface radiation budget, d) surface sensible heat flux, e) surface latent heat flux, f) specific humidity in the boundary layer (BL), g) relative humidity in the BL and h) low cloud cover represented by linear regression of the period 1979–2023. Trend values represent area-weighted means with respect to land globally.

https://doi.org/10.5194/egusphere-2026-1654
Preprint. Discussion started: 2 April 2026

3.4 Trends in ERA5 radiation, heat flux, humidity, and low cloud cover over land globally

Based on linear regression, trends in ERA5 annual quantities/parameters over the period 1979–2023 are presented in Fig. 5. The numbers corresponding to the figures represent mean trend values for land globally. The trends are statistically significant at the 95% confidence level, with p-values <<0.05, except for latent heat flux and specific humidity (p-values of 0.084 and 0.24, respectively). The latter is thus explained by trends of opposite signs over land globally (Fig. 5e and 5f). Figure 5a shows strong warming over land, particularly in the Northern Hemisphere. This aligns with widespread strong increases in TOA net solar radiation, supported by CERES and CLARA-A3 (Fig. 1b and 2b, respectively). The weak warming over South Asia, shown in Fig. 5a, coincides with negative trends in TOA net solar radiation from ERA5 and CERES. In addition, ERA5, CERES, and CLARA-A3 show decreases in TOA and surface upward terrestrial radiation over this region, while positive trends dominate over land globally (Fig. 1-3). Relatively strong increases in sensible heat flux appear over large parts of global land in Fig. 5d, while also here with the exception for South Asia. The increases in exchange of dry heat between the land surface and the air have occurred along with strong increases in latent heat flux over the oceans (Fig. 5e). Widespread decreases in relative humidity and low cloud cover are found over land areas (Fig. 5g and 5h, respectively), while an increase in relative humidity appears over South Asia. The latter is also shown in the results from HadISDH (Fig. 3b). Positive trends in low cloud cover appear however over large parts of the oceans.

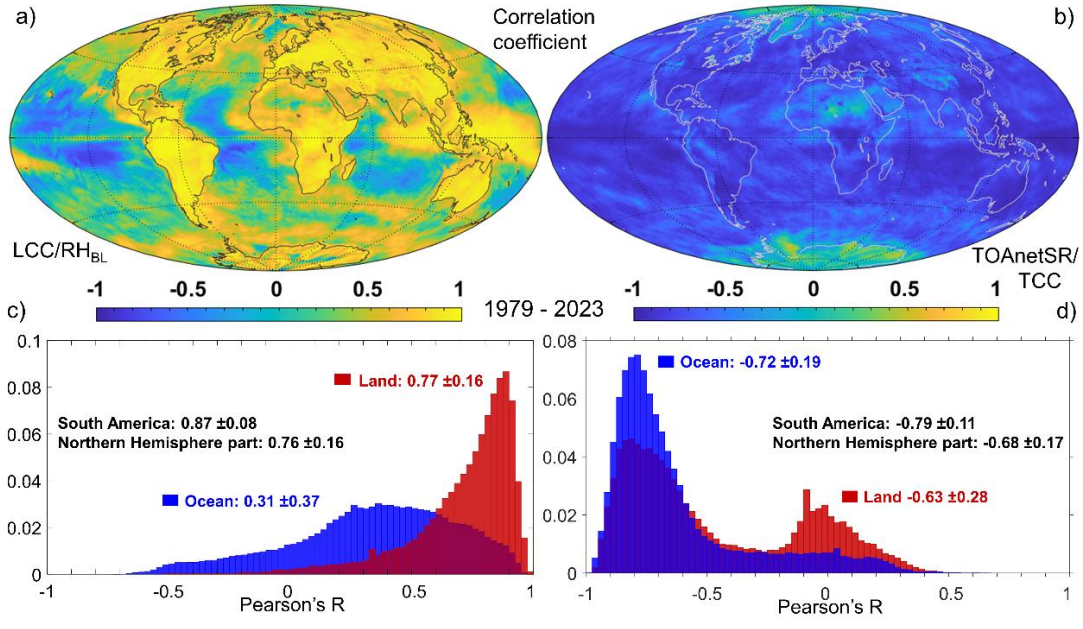

Figure 6. Scenes of Pearson's correlation between annual a) relative humidity in the boundary layer (RH_{BLH}) and low cloud cover (LCC) and b) total cloud cover (TCC) and net top of the atmosphere solar radiation (netTOAsrof) of the period 1979 – 2023. c) and d) Normalized distribution Pearson's correlation coefficient from results presented in panel a) and b), respectively, for land and ocean globally with corresponding mean values presented. Mean values of correlation coefficient are also presented for South America and the areas in the Northern Hemisphere (43°N-90°N, 180°W-180°E).

https://doi.org/10.5194/egusphere-2026-1654
Preprint. Discussion started: 2 April 2026

Figures 6a and 6c show results of Pearson's correlation coefficient (R) between low cloud cover (LCC) and relative humidity in the boundary layer (RH_{BL}) of the period 1979–2023. The strongest correlation appears on the whole over land, where 95% of the pixel values are statistically significant at the 95% confidence level. The present results are in line with the study carried out by Liu et al. (2023), based on an empirical orthogonal function analysis on 42 years of ERA reanalysis, who found a relatively high mean positive correlation and narrow spread over land globally, 0.69 ±0.18, between near surface relative humidity and total cloud cover during the period 1979–2020. They conclude that decreased cloud cover over land is explained by a reduction in near-surface relative humidity. Furthermore, Fig. 6b and 6d show results of R between net TOA solar radiation and total cloud cover of the period 1979–2023. Two modes appear in the distribution of R for global land, where values around zero are related to areas with high surface albedo such as Sahara, Greenland and Antarctica. For land and ocean, 68 and 87% of the pixel values, respectively, are statistically significant at the 95% confidence level, according to anti-correlation between the variables.

3.5 Regional trends in ERA5 quantities/parameters

We continue to discuss results from ERA5, with a focus on South America and land areas in mid- and high latitudes in the Northern Hemisphere (43°N–90°N, 180°W–180°E). Figure 5b shows strong positive trends in TOA net solar radiation over both regions from 1979, on the whole also for sensible heat flux. At the same time, strong negative trends in relative humidity in the boundary layer and low cloud cover appear over both regions. The mean Pearsons's correlation coefficients between the latter variables are shown in Fig. 6a and 6c, where all pixel values corresponding to both regions are statistically significant at the 95% confidence level. The decreases in low level clouds are on average 9 and 3% from 1979 to 2023 for South America and the areas in the Northern Hemisphere, respectively (Fig. 7h and 8h). In addition, statistical significance between relative humidity and total cloud cover is found for 98% of the pixel values for both regions, where the mean correlation coefficients are 0.78 ±0.12 and 0.68 ±0.15 for the former and latter areas, respectively. Weaker decreases in total cloud cover with 5 and 2% during the investigation period, compared to changes in the low cloud cover, are found for South America and the Northern Hemispheric case, respectively. These trends are in any case statistically significant at the 95% confidence level.

Furthermore, mean negative correlation coefficients between total cloud cover and TOA net solar radiation for the present two regions are shown in Fig. 6b and 6d, where the stronger anti-correlation appears for South America. 100 and 94% of the pixel values for South America and the areas in the Northern Hemisphere, respectively, are statistically significant at the 95% confidence level. Trends of opposite signs in specific humidity between the two regions are nevertheless obvious in Fig. 5f. The warming in the Northern Hemisphere is on the whole stronger than in the Southern Hemisphere (Fig. 5a).

Figures 7 and 8 show trends with corresponding confidence intervals in ERA5 quantities and parameters over the investigation period, averaged for South America and the land areas in the Northern Hemisphere. The low p-values indicate strong increases

https://doi.org/10.5194/egusphere-2026-1654
Preprint. Discussion started: 2 April 2026

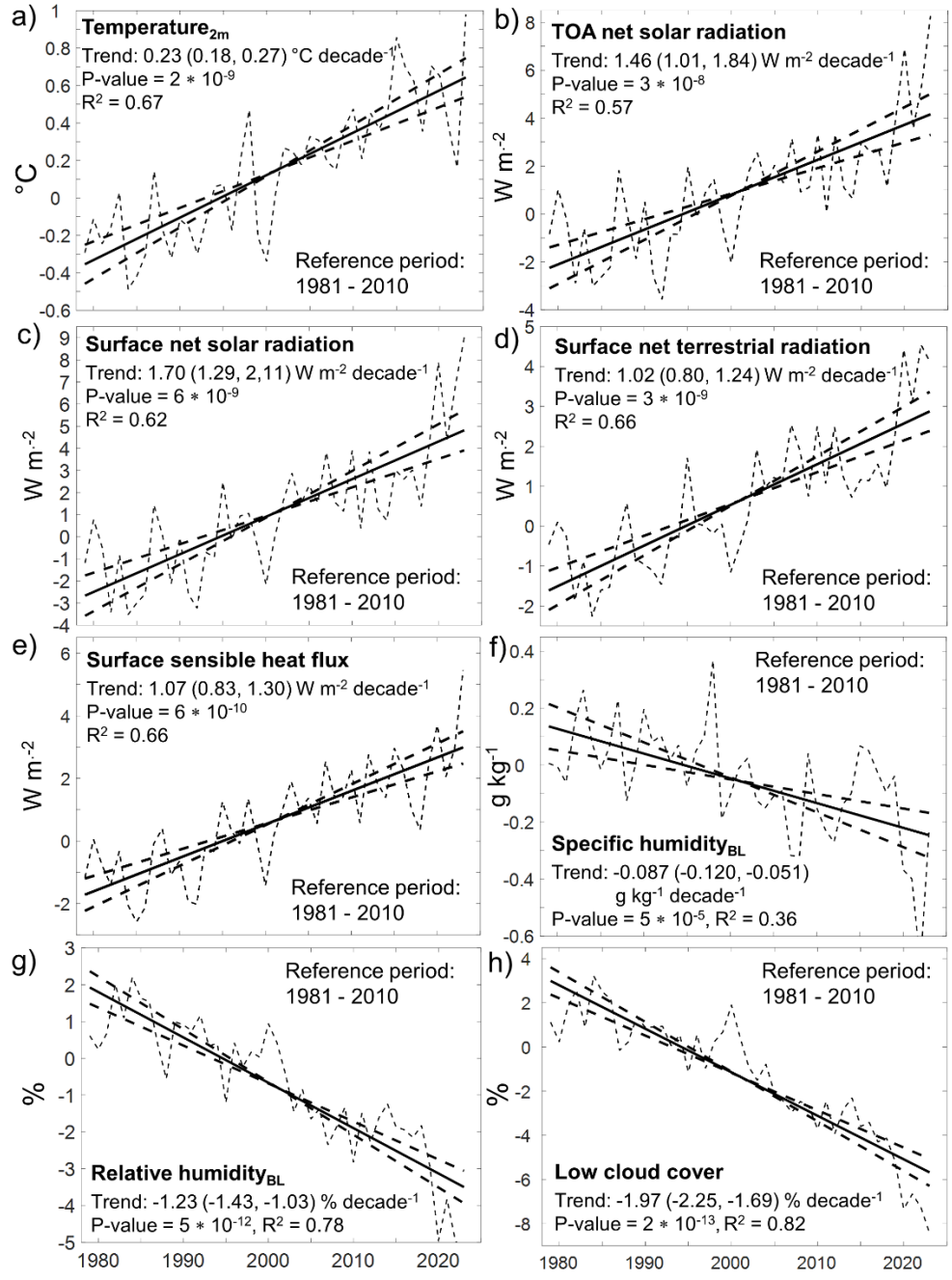

Figure 7. Heavy solid and dashed lines denote linear regressions and corresponding 95% confidence intervals, respectively, of annual anomalies (light dashed lines) in ERA5 parameters obtained over area-weighted South America of the period 1979 – 2023 compared to mean of the 1981 - 2010. Mean trend values with 95% confidence bounds are presented, where corresponding p-values are obtained by Mann-Kendall test at the 95% confidence interval.

https://doi.org/10.5194/egusphere-2026-1654
Preprint. Discussion started: 2 April 2026

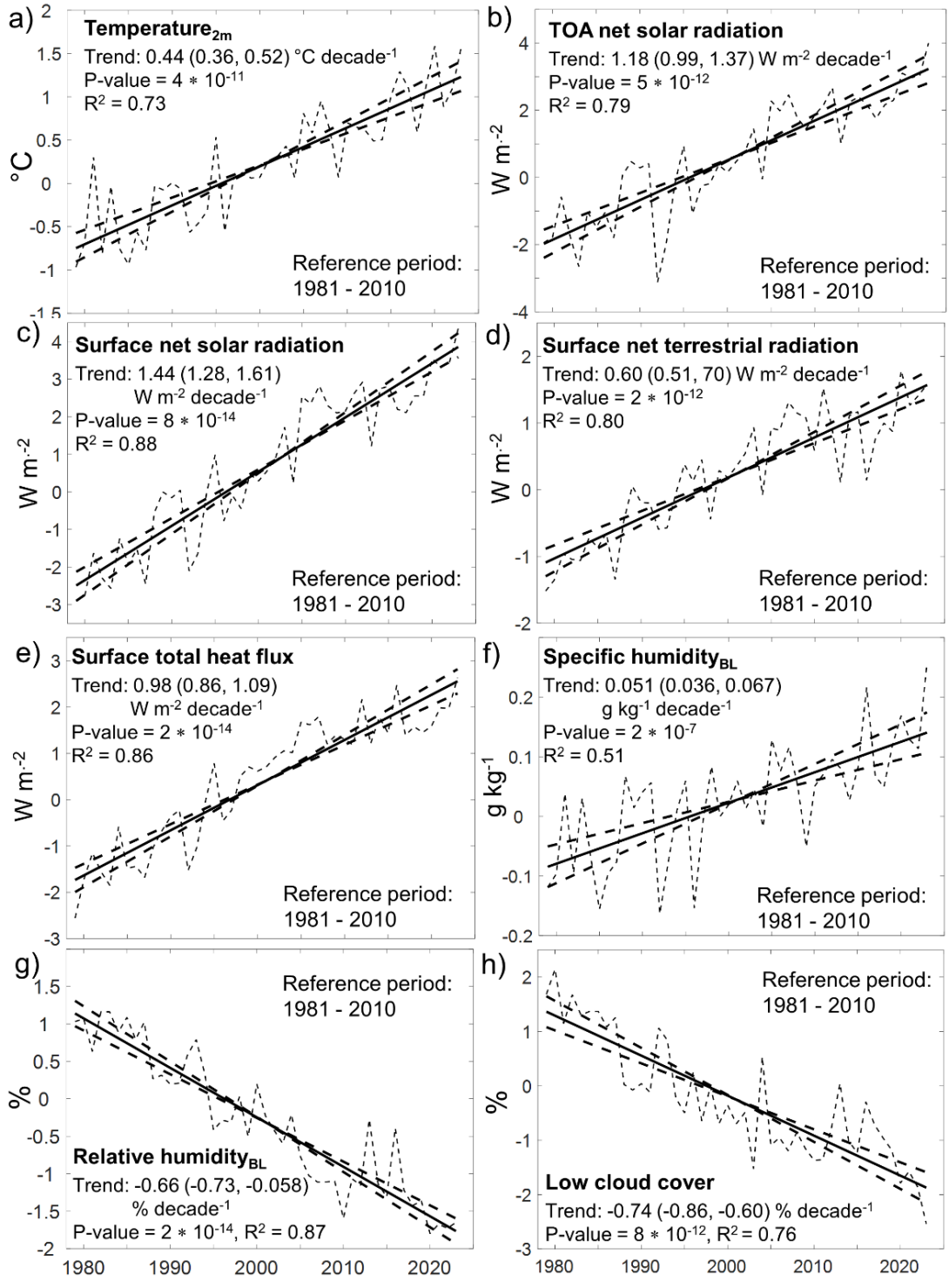

Figure 8. The same as in Fig.7, while here with respect to areas in the northern hemisphere and surface total heat flux is presented in e) instead of surface sensible heat flux.

https://doi.org/10.5194/egusphere-2026-1654
Preprint. Discussion started: 2 April 2026

or decreases based on linear regressions for both regions. The results obtained for 2023 reinforce the trends observed in South America for all cases, with the exception of specific humidity (Fig. 7f). The long-term negative trends in both relative and specific humidity indicate a depletion of water supply in the latter region. Instead of a positive water vapour response in the boundary layer to surface air temperature long-term opposite trends are found for South America (Fig. 7a and 7f). This appears also for southwestern North America and some other regions on Earth (Fig. 5f and 5g). The total column water vapour response in percent to temperature from 1979 to 2023, averaged for South America according to Clausius Clapeyron relationship between uptake of moisture due to temperature increase (7 % K^{-1}), is close to zero (-0.16%). Even so, statistically significant trends in total column water vapour of opposite sign, with positive and negative responses to temperature of 2 and -3%, appear north and south of 10°S in South America, respectively. Fig. 9 shows that negative responses appear as well for southwestern North America, central Asia and tropical Africa, and positive responses lower than the Clausius Clapeyron relationship appear over large land areas. A mean positive response of 3.0% appears for the areas in the Northern Hemisphere.

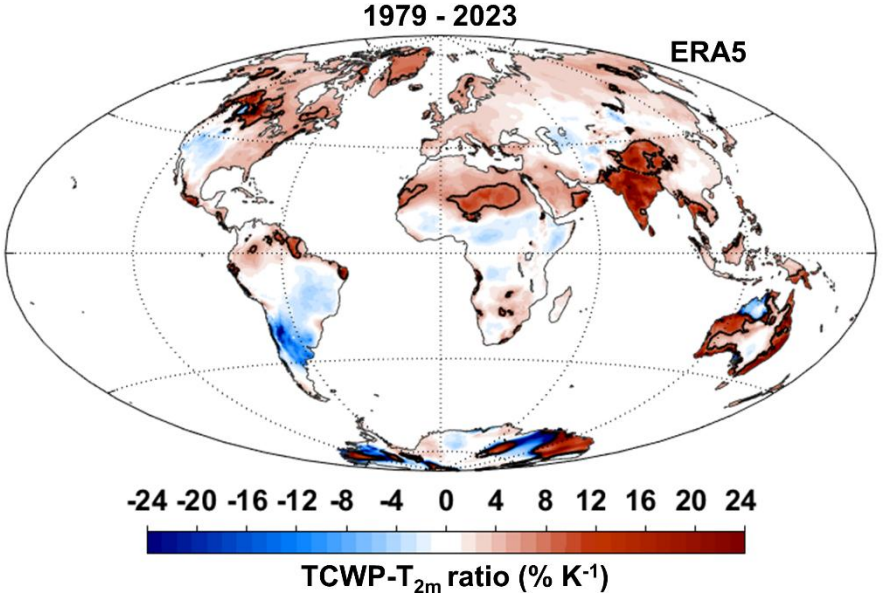

Figure 9. Trends in the ratio between ERA5 total column water vapour (TCWP in %) and temperature at 2 m height (T_{2m} in kelvin (K)) of the period 1979 – 2023, where the black solid line denotes 7 % per K according to Clausius-Clapeyron equation between uptake of moisture in the air due to warming.

Depletion of water supply has affected latent heat flux that is associated with a statistically significant negative trend of -0.37 W m^{-2} $decade^{-1}$ for South America, although minor increases appear regionally in Fig. 5e. In addition to a strong increase in mean sensible heat flux, with 1.1 W m^{-2} $decade^{-1}$ (Fig. 7e), substantially reduced evaporative cooling has consequently occurred in South America during the latest four decades. The increase in the Bowen ratio between sensible and latent heat flux with 15% between 1979 and 2023 based on linear regression, is statistically significant. Specific humidity has however increased over the current Northern Hemisphere region, while relative humidity and low cloud cover have decreased (Figure 8). This is

https://doi.org/10.5194/egusphere-2026-1654
Preprint. Discussion started: 2 April 2026

probably driven by the differentiation of warming in the oceans and in the air over land, which causes the air to be further away from saturation at present. Figure 8e shows a strong increase in mean total heat flux over the areas in the Northern Hemisphere, where the positive trend in sensible heat flux, 0.54 W m^{-2} $decade^{-1}$, is higher than 0.43 W m^{-2} $decade^{-1}$ for latent heat flux. A statistically significant positive trend in the Bowen ratio is found, with an increase of 6.5% since 1979. Strong positive trends in surface net terrestrial radiation, shown in Fig. 7d and 8d, mean a stronger increase in upward radiation than an increase in downward radiation. The cooling in infrared has been more efficient over South America compared to the present land areas in the Northern Hemisphere (Fig. 7c, 7d, 8c, and 8d). This is in line with a weaker mean trend in surface radiation budget, 0.68 (0.44, 0.92) W m^{-2} $decade^{-1}$, since 1979 over the current continent compared to the latter areas, 0.84 (0.73, 0.94) W m^{-2} $decade^{-1}$. These values with corresponding 95% confidence bounds are, based on an unpaired Wilcoxon rank sum test, statistically significant different at the 99% confidence level. The results are in line with a stronger warming that has occurred in the Northern Hemisphere than in South America (Fig. 7a and 8a). The ERA5 surface energy budget is, however, not in accurate balance for the areas in the Northern Hemisphere since the trend in total heat flux is 16% higher than the trends in radiation budget, but only 2% higher for South America.

Furthermore, Fig. 10 shows decreases in surface upward solar radiation, depending on seasons, at middle and high latitudes by comparing the rates of mean values (in percent) of the periods 2014–2023 and 1979–1988. The strong decreases that appear in the Arctic basin in late summer and autumn are explained by a decline in sea ice (not shown). A shorter period with snow covers likely explains decreases in the albedo over land. The summer period, June-August, shown in the figure, is associated with minor changes in surface upward solar radiation over land. Decreases in the present land albedo are in line with negative trends in snow cover extent, from NOAA visible satellite-based analysis, in spring of the period 1967–2020 for Arctic terrestrial areas (Mudryk et al., 2021). Furthermore, an updated ensemble of six gridded snow products for snow extent reveals strong negative trends in early winter and spring during the period 1981–2018 in the Northern Hemisphere (Mudryk et al., 2020). Trends are found also in this study to be near zero during the summer, since there is very little land area with snow cover.

https://doi.org/10.5194/egusphere-2026-1654
Preprint. Discussion started: 2 April 2026

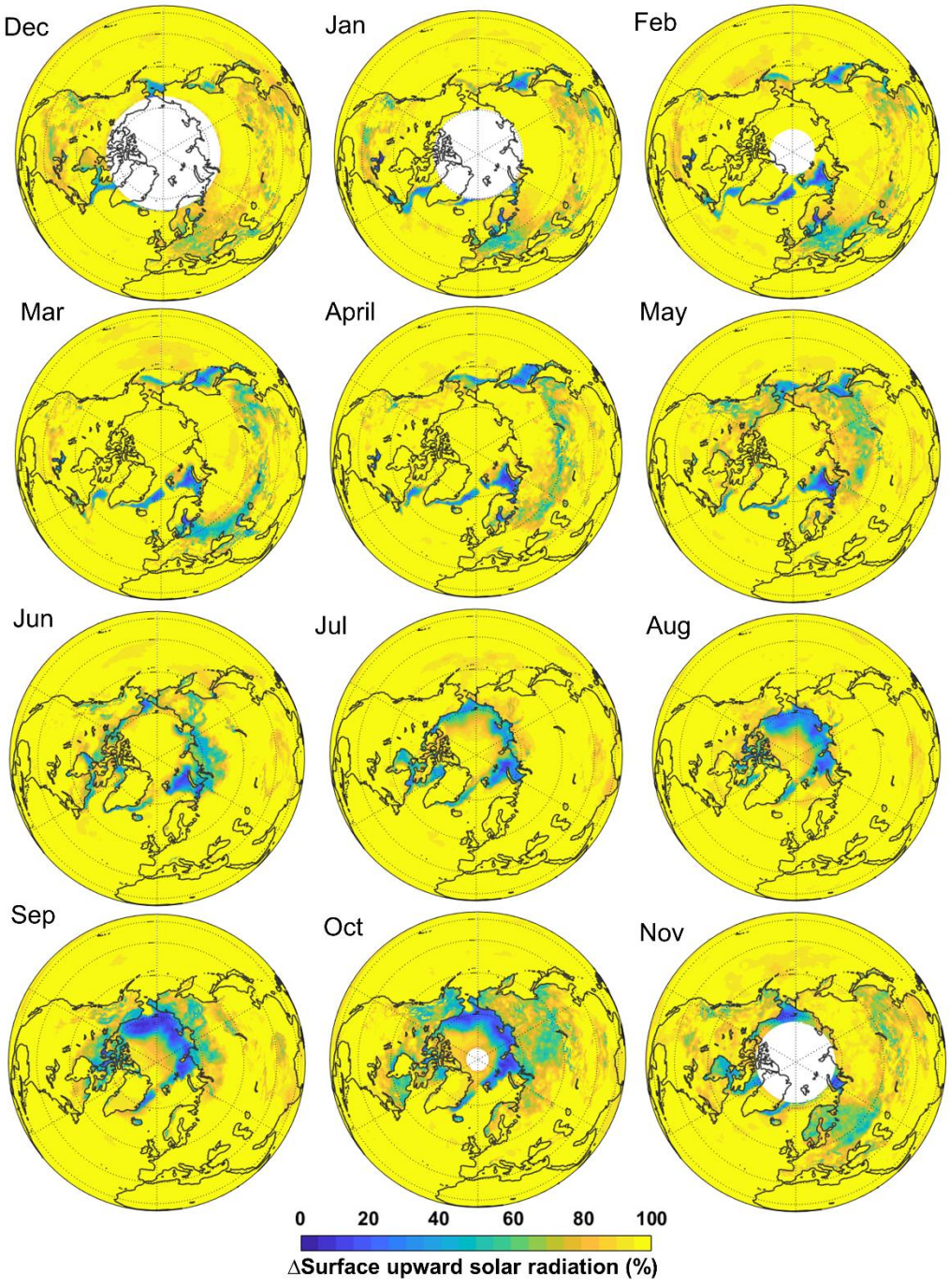

Figure 10. Changes in annual ERA5 surface upward solar radiation in the Northern hemisphere, obtained by comparing the rates of mean values (in percent) of the periods 2014-2023 and 1979-1988. No data are available during the polar night, denoted with white colour.

525

https://doi.org/10.5194/egusphere-2026-1654
Preprint. Discussion started: 2 April 2026

3.6 Global and regional trends in total annual precipitation amount over land

Figures 11a and 11b show climatology scenes of total annual precipitation (in meters) averaged over the period 1983–2023 for ERA5 and GPCP, respectively, where the highest values on the whole appear in the tropics. Comparisons of ERA5 and GPCP total annual precipitation amounts in percent for the period 2014–2023 compared to the mean of 1983–1992 are shown in Fig. 11c and 11d, respectively. The figures show opposite trends in the ERA5 and GPCP precipitation over areas in Asia and Africa, as well as in North America. Even so, decreases in annual precipitation appear over large parts of South America, Africa, and Australia, and in southwestern North America for both ERA5 and GPCP. Stronger trends appear, however, for the former data set. The negative trends coincide with decreases in ERA5 latent heat flux and specific humidity shown in Fig. 5e and 5f, respectively. Positive trends are found for both ERA5 and GPCP as well; for example, in the wetter northern South America and Australia, eastern US, and over part of the Indian subcontinent (Fig. 11a and 11b). The negative trends in precipitation appear over some dry regions on Earth for both ERA5 and GPCP, such as southwestern North America, a large part of Australia, northern Africa, and Middle East.

Statistically significant decreases in ERA5, GPCP, and GPCC total annual precipitation over South America during the period 1983–2023 are shown in Fig. 11e. Statistically significant positive trends in GPCP and GPCC precipitation are shown in Fig. 11f for the Northern Hemisphere areas, while the ERA5 trend is substantially weaker and not significant. This is explained by the difference in the sign of the trends that appear between the ERA5 and GPCP/GPCC over Asia and North America (Fig. 11c and 11d, respectively). Pearson's correlation between ERA5 and GPCP total annual precipitation amount over the period is 0.74 for South America, while substantially lower, 0.46, for the Northern Hemisphere areas. The ERA5 total annual mean precipitation of the current period is 11% and 10% higher than GPCP for South America and the Northern Hemisphere areas, respectively.

https://doi.org/10.5194/egusphere-2026-1654
Preprint. Discussion started: 2 April 2026

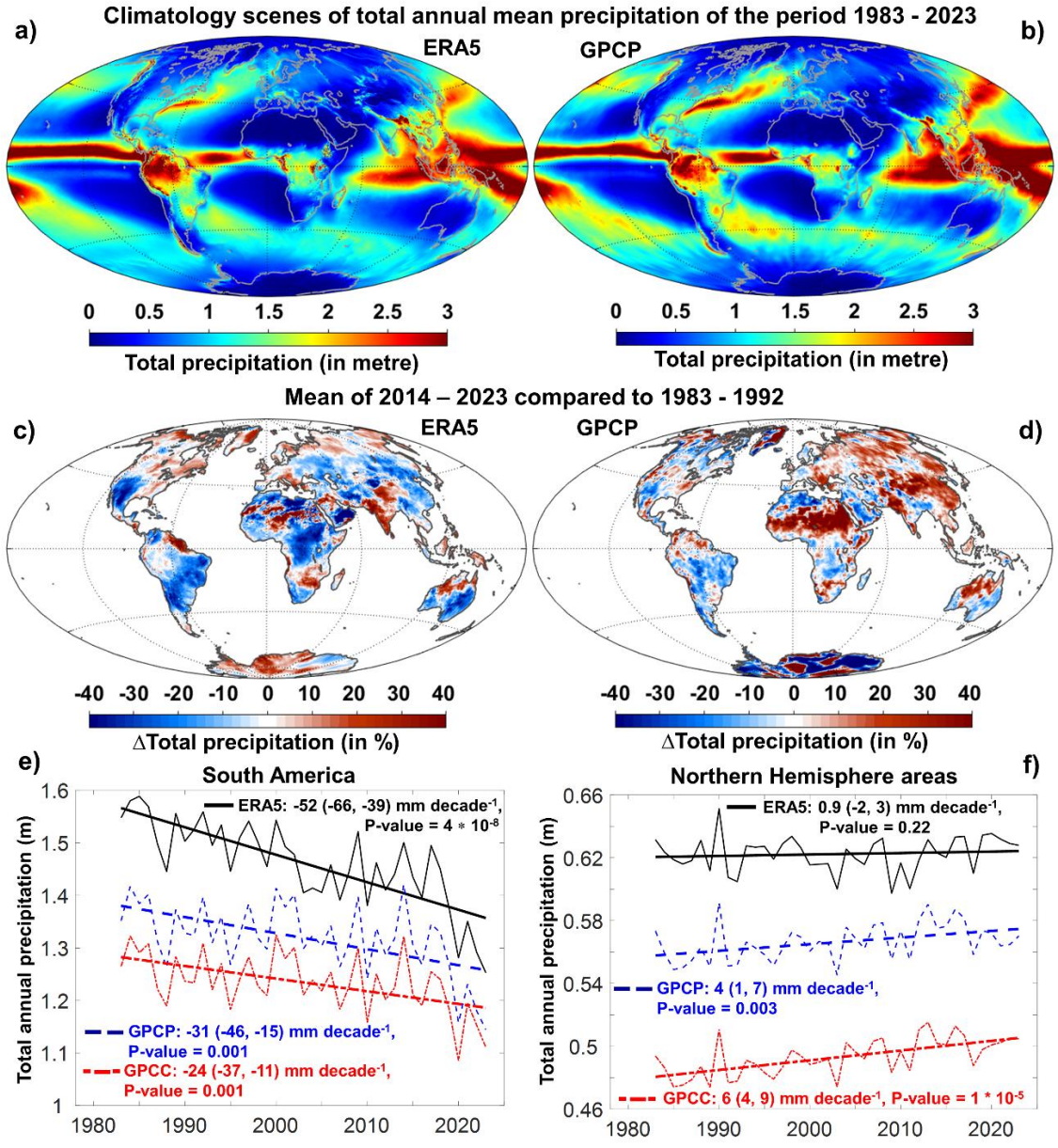

Figure 11. Total annual mean precipitation amount in metre (m) of the period 1983–2023 for a) ERA5 and b) GPCP. Total annual mean precipitation amount for 2014–2023 compared to 1983–1992 in percent (%) for c) ERA5 and d) GPCP. Trends in total annual precipitation of the period 1983–2023 for ERA5, GPCP and GPCC of the period 1983–2003 for e) South America and f) Northern Hemisphere areas. Heavy solid black, dashed blue and dashed-dotted red lines denote linear regressions of total precipitation for ERA5, GPCP and GPCC, respectively, over area-weighted e) South America and d) Northern Hemisphere areas.

https://doi.org/10.5194/egusphere-2026-1654
Preprint. Discussion started: 2 April 2026

Figure12a shows GPCC total annual precipitation amount for the period 2014–2023 compared to the mean of 1983–1992. The positive and negative trends over land globally are very similar to the results from GPCP shown in Fig. 11d. Even so, in the view of the latest version of GPCP satellite/gauge space (0.5°) and time homogeneity since 1983, Fig. 12b shows that the GPCC gauges don't exist at high latitudes in the Northern Hemisphere and for large parts of Africa and Australia. In addition, the gauges are relatively sparse in large parts of South America. Gauge-based estimates of precipitation in these regions have therefore to rely on interpolation of limitation in data, reducing the quality of the results.

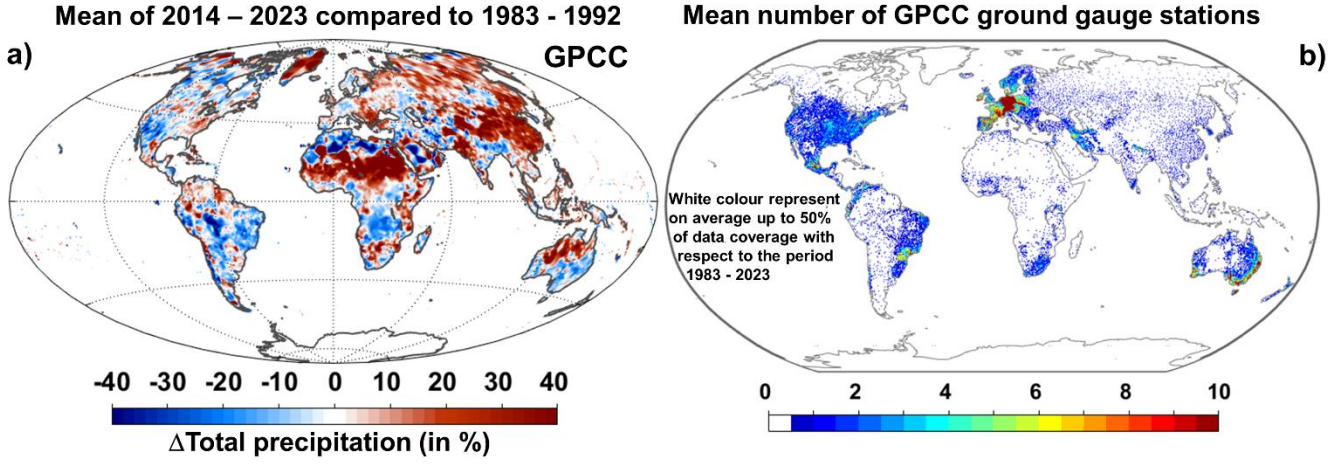

Figure 12. a) GPCC total annual mean precipitation amount for 2014 – 2023 compared to 1983 – 1992 in percent (%). d) Number of GPCC ground gauge stations in 0.5° x 0.5° grids averaged for 1983 – 2023, in view of GPCP Version 3.3 satellite/gauge space (0.5°) and time homogeneity since 1983.

3.7. Long-term surface air temperature anomalies over land and ocean globally

Figure 13 shows trends in ERA5 surface air temperature anomalies during the period 1940 – 2024 compared to the mean of the reference period 1850 – 1900, separated for land and ocean. The temperature values for the 1850 – 1900 period (pre-industrial) that have been subtracted to obtain the anomalies are: 7.9°C for land and 15.8°C for ocean. These estimates are based on offset values, 1.3 °C and 0.7 °C for land and ocean, respectively, between the periods 1850 – 1900 and 1991 – 2020 from IPCC (2021). This is the most recent version of the pre-industrial level, which has been updated following recent IPCC AR6 assessments. The changes in AR6 surface air temperature over land and ocean globally for 1850 – 2020 are also presented in Figure 13. The figure shows a steady increase in ocean-land warming contrast since around 1980.

https://doi.org/10.5194/egusphere-2026-1654
Preprint. Discussion started: 2 April 2026

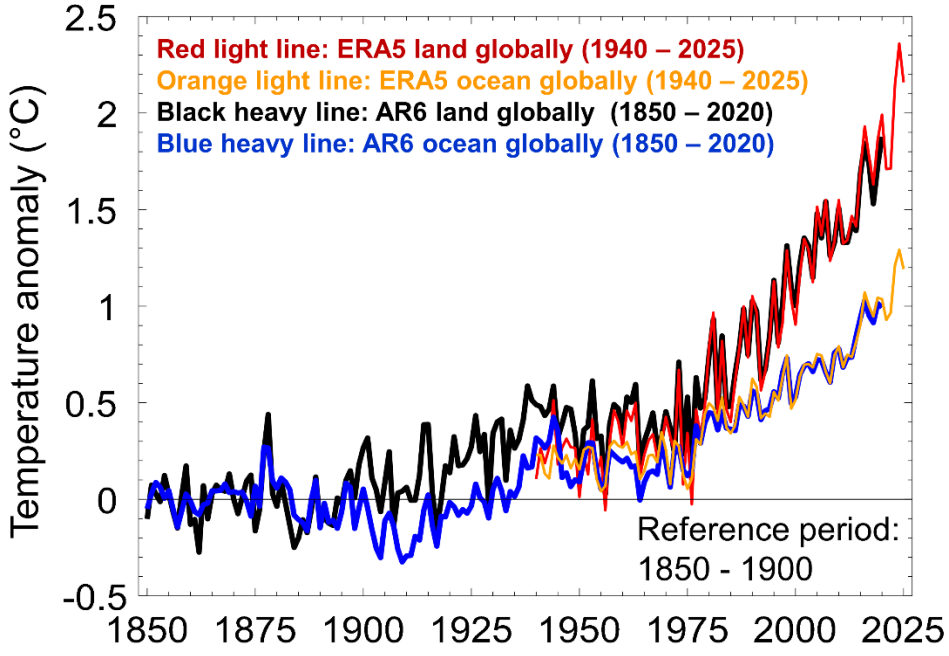

Figure 13. shows trends in ERA5 surface air temperature separated for land and ocean globally during the period 1940–2025 compared to the mean of the reference period 1850–1900. The latter is the most recent version of the pre-industrial level, which has been updated following recent IPCC assessments. Changes in surface air temperature over land and ocean globally during the period 1850 – 2020 from Figure 2.11c in Chapter 2.3.1.1.2 in IPCC AR6, 2021, are also presented. The figure shows a steady increase in ocean-land warming contrast since around 1980.

4 Discussion and summary

Uncertainties in absolute calibration and the algorithms used to determine Earth's radiation budget from satellite measurements are too large at present to enable Earth's energy imbalance to be accurately quantified (Loeb et al., 2018). Even so, in comparison with in-situ ocean heat content data, Loeb et al. (2021) conclude that the CERES trend toward an increase in Earth's energy budget is robust. Based on CERES observations, Loeb et al. (2024) found that the Earth's energy imbalance has doubled from 0.5 ± 0.2 Wm^{-2} during the first ten years of this century to 1.0 ± 0.2 Wm^{-2} during the period 2013–2022. Reasonable agreements in positive trends in solar radiation over land globally during the period 2001–2003 between ERA5 and CERES are on the whole found in the present study (Table 1). A large disagreement appears, however, for surface net terrestrial radiation in addition to unrealistic trends in CERES skin temperature over a large part of South America (Sect. 3.1). The comparison of ERA5 and CLARAA3 trends in surface net terrestrial radiation, considering the CERES data record and period 1986–2023, shows nevertheless better agreement (Table 1 and Fig. 2i, respectively). Good agreement between ERA5 and CLARA-A3 appears for TOA upward solar and terrestrial radiation since 1982 (Fig. 2c and

https://doi.org/10.5194/egusphere-2026-1654
Preprint. Discussion started: 2 April 2026

Table 2). The ERA5 surface energy budget is associated with small uncertainty considering trends over the period 1979–2023 for South America, but somewhat larger uncertainty appears for the areas in the Northern Hemisphere (Sect. 3.5). The results from ERA5 radiation quantities are useful to provide qualitative statements about spatial variability and global and regional changes over time.

Statistically significant positive trends in TOA solar radiation from ERA5, CERES, and CLARA-A3 are on the whole large over land globally, where the supply of solar energy at the ground has occurred successively during the last four decades. The TOA annual solar radiative forcing is 1.3 and 1.5 W m^2, averaging over land globally since 2001, for ERA5 and CERES, respectively. The increase in annual skin temperature is 0.84 °C for ERA5 and 0.75 °C for CERES during the same period. Furthermore, the decreases in TOA upward solar radiation are 3.6 and 3.7 W m^{-2} over land globally since 1982 for ERA5 and CLARA-A3, respectively. The increase in ERA5 annual temperature at 2 m height over land globally is 1.4 °C since 1979, and even stronger warming, with 2.0 °C, has occurred over land in the Northern Hemisphere.

The increase in solar radiative forcing has occurred in addition to the supply of infrared energy due to the enhanced greenhouse effect by anthropogenic greenhouse gases. The increase in ERA5 surface net solar radiation is about 7 W m^{-2} since 1979 for both South America and the areas in the Northern Hemisphere (Fig. 7c and 8c, respectively). This large supply of solar energy is consistent with strong decreases in CLARA-A3 TOA and ERA5 TOA upward solar radiation during 1982 – 2023 over South America (Table 2). Lower decreases in reflected solar radiation of 4.1 and 5.3 W m^{-2} for CLARA-A3 and ERA5, respectively, appear however during the same period for the areas in the Northern Hemisphere. This may be explained by decline in snow cover (Sect. 3.5). Increases in ERA5, CERES, and CLARA-A3 surface net terrestrial radiation are found as well over large parts of the Earth (Fig. 1g, 1h, 2g and 2h), suggesting that land surfaces have been efficient in cooling in the infrared. The latter is probably explained by decreases in low cloud cover (Fig. 5h) and total cloud cover (Sect. 3.5). Loeb et al. (2024) found that absorbed solar radiation in a global perspective has partially been offset by an increase of 0.4 ±0.25 W m^{-2} in outgoing terrestrial radiation during the last two decades. Furthermore, a weaker warming in South America than over land at middle and high latitudes in the Northern Hemisphere since 1979 is in line with more efficient cooling in infrared over the former continent. In addition to decreases in low level clouds as well as total cloud cover over South America reduction in total column water vapour may also have contributed to cooling in the infrared, at least over part of the continent (Fig. 9). This is relevant also for western US, central Asia and tropical Africa. One region on Earth, South Asia, deviates from the general trend pattern considering TOA net solar radiation, surface net terrestrial radiation, sensible and latent heat flux, and relative humidity (Figure 5). Figure 9g shows as well a strong positive response in total column water vapour to temperature from 1979 to 2023. The strongest increase in specific humidity is thus found in this region. Reduced solar radiative forcing is likely explained by high aerosol loading in this region, while these have strongly been reduced at other regions on Earth. Vegetation greening may as well have contributed to a cooling effect and offset of warming in this region during the period 2001–2018 (Li et al., 2023), in line with the present positive trends in heat fluxes, relative humidity and specific humidity. However, some of the greening

https://doi.org/10.5194/egusphere-2026-1654
Preprint. Discussion started: 2 April 2026

has reversed to a browning i.e. at higher northern latitudes (e.g. Phoenix et al., 2025) highlighting the complexity and spatiotemporal heterogeneity of surface albedo changes (Myers-Smith et al., 2020).

Increases in TOA net solar radiation over land suggests decreases in cloud albedo. Related to Earth's energy imbalance and decline in clouds, Loeb et al. (2024) found that increases in absorbed solar radiation of the planet since 2000 are mainly explained by reduced cloud reflection in both the Northern Hemisphere and Southern Hemisphere. There is a strong indication that decreases in the clouds are related to decreases in relative humidity over land. For South America, both boundary layer relative humidity and specific humidity from ERA5 have on the whole decreased over the last four decades. The strong supply of ERA5 surface net solar radiation since 1979 and the general enhanced greenhouse effect make the surface drier. In addition, the strong decreases in ERA5 and GPCP total annual precipitation for South America and other regions on Earth (Fig. 11) indicate perturbed water balance at the land surface. The present results are beyond the outcomes from the study by Manabe et al. (2019), who explain changes in the water balance in relatively arid regions associated with low amounts of precipitation due to increases in purely IR-radiation (Sect. 1). A strong increase in surface sensible heat flux has consequently appeared in South America, and latent heat flux is associated with a trend of opposite sign over large parts of the continent. This has, on the whole, led to a shift in heat flux but also reduced evaporative cooling and likely contributed to the increase in the warming contrast between land and ocean (Fig. 13). Oceans have unlimited water to evaporate and can therefore efficiently cool in a warming climate by evaporating more and more water.

Evaporation thus increases due to global warming, a consequence of the Clausius-Clapeyron relationship (Allan et al., 2020; 2022). Strong positive trends in latent heat flux also appear over large parts of the oceans (Fig. 5e), while Fig. 5h shows a diverse signs of the trend in low cloud cover. Allan et al. (2020) suggests that changes in water vapour over global land have a weaker thermodynamic response. They claim this according to relative humidity that is expected to decrease due to stronger ocean-land warming contrast (Byrne and O'Gorman, 2018), which in turn is amplified by land surface feedbacks associated with land hydrology response to climate change (Berg et al., 2016). The present study finds an extreme long-term opposite trend between water vapour in the boundary layer and surface air temperature for South America, as well as for other land areas on Earth. When considering total column water vapour a negative response according to the Clausius-Clapeyron equation is found as well (Fig. 9) over large parts of South America, western US, central Asia and tropical Africa, under the present rapid global warming. More of the extra radiation going into the land surface during the recent warming climate has to a larger degree be dissipated through the exchange of dry heat and longwave radiative cooling rather than evapotranspiration. Reduced evaporation and evaporative cooling over South America, in addition to increases in sensible heat flux and atmospheric warming, tends to inhibit cloud formation. This causes further drying of the land surface.

Measurements in Amazon rainforest show that replacement of forest by pastures leads to a decrease in evaporation and consequently an increase in sensible heat flux (Gash and Nobre, 1997). Due to this landscape change the authors report on an

https://doi.org/10.5194/egusphere-2026-1654
Preprint. Discussion started: 2 April 2026

increase of surface albedo from approximately 0.13 to approximately 0.18 and an increase in net longwave radiation. The latter since deforestation leads to higher surface temperature. Both effects lead to a decrease in the surface radiation budget of 11%. Luo et al. (2024b) and Næss et al. (2025) found a reduction in the clouds due to deforestation. Deforestation-induced reduction in cloud cover was found to warm the climate and partially counteract, with respect to global average, the cooling effects of increased surface albedo (Luo et al., 2024b). The overall biophysical effect of deforestation leads to cooling in the boreal zone. In tropical deforested areas, however, surface warming was found due to the prevailing impact of evapotranspiration, although alterations in surface albedo partially counteract the warming (Luo et al., 2024b). Deforestation in the Amazon has resulted in a loss of approximately 20% of the rainforest biome since 1985 (Quintanilla et al. 2025; Artaxo et al. 2022; Flores et al. 2024). The net of land-use change in the Amazon is thus a warming effect and relevant for about 10% of the area in South America. Even so, climate and land-use changes, particularly deforestation, have increased rainfall variability in the region during recent decades (Li et al., 2025). The authors found compensatory effects of deforestation on downwind precipitation in Brazilian breadbaskets. Enhanced moisture transport was found upwind, such as from Amazonia and from the Atlantic Ocean.

The strongest warming during the last four decades, based on ERA5 data, is thus found over the land areas in the Northern Hemisphere. A similar rate in the increase of CERES skin temperature since 2001, 0.43 °C per decade, supports this finding. Decreases in ERA5 surface upward solar radiation at the middle and high latitudes in the Northern Hemisphere, depending on the season, suggest a decline in sea ice (not shown) and likely a shorter period with snow cover over land at present. The latter finding is in line with previous studies (Mudryk et al., 2020; 2021). This has likely contributed to the on-going rapid warming. Furthermore, positive trends in ERA5 specific humidity are found on the whole in the Northern Hemisphere, simultaneously as relative humidity has decreased since 1979. Present results from HadISDH support these findings. The increases in water vapour over this region are likely explained by advection from the warmed oceans (Wang et al., 2023). Instead of favouring cloud formation at present, the enhancement in water vapour over the areas in the Northern Hemisphere is suggested to contribute to an even stronger greenhouse effect. Even if specific humidity and latent heat flux have increased in this region, drier surface conditions and consequently a decline in the supply of water vapor due to global warming can in any case not be excluded as a contributing factor for the decrease in relative humidity. The decline in human aerosols over the eastern US and in Europe since around 1980 (Glantz et al., 2022; Smith et al. 2011b) to nearly natural levels has led to increases in absorbed solar radiation at the surface and exposed greenhouse warming. This has likely contributed to increases in sensible and latent heat fluxes and in specific humidity over these regions. A statistically significant positive trend in Bowen ratio is found for the Northern Hemisphere case (Sect. 3.5), which nevertheless indicates an increase in evaporation demand. Figure 5 shows as well that latent heat flux decreased simultaneously as sensible heat flux increased in the southwestern North America and southern Europe, thus, similar to the changes in South America. Decrease in precipitation over the latter regions is an additional indication of stress on the terrestrial water cycle. A decline in ERA5 specific humidity appears as well in the southwestern North America, which aligns with the latter finding and results from HadISDH. Martens et al. (2020) found that ERA5 reanalyses of surface heat fluxes of the period 1983 – 2018 are overall of high quality, in comparison with different reference

https://doi.org/10.5194/egusphere-2026-1654
Preprint. Discussion started: 2 April 2026

data sets and modelling tools. The authors found improvement in the ERA5 latent heat flux, including a better quality of the surface energy partitioning, compared to the previous ERA-Interim reanalysis. Even so, overestimation of surface latent heat flux was found over land.

Global climate models estimate the relative humidity feedback to be close to zero, although a spread of 0.06 W m^{-2} among the models is circumscribed to the tropics (Sect. 7.4.2.2 in IPCC, 2021). However, the theoretical expectation of a constant tropospheric relative humidity over land under global warming lacks unequivocal observational evidence (Douville et al., 2022). The present study finds decreases in relative humidity over land globally that coincide with rapid warming compared to the weaker warming over the oceans. Even greater climate change is expected in the coming decades if internal variability associated with atmospheric weather systems remains the same or changes don't act to decrease the rate of heat uptake. Tselioudis (2025) found, based on past 24 years of satellite observations, that the storm cloud zones, mainly over the oceans, have been contracting at a rate of 1.5 – 3% per decade. This has led to more absorption of solar radiation at the Earth's surface. A poleward shift of the storm tracks with climate change is suggested to be caused by a balance between increasing and decreasing meridional temperature gradient in the upper and lower troposphere, respectively (Woolings et al., 2023). The present study suggests that positive feedbacks initiated by global warming must be considered in predicting future climate change over global land areas. Natural internal variability not investigated in the present study may also play a role for these changes, although the contribution is expected to subside and leave the observed long-term warming unaffected (Goessling et al., 2024).

5 Conclusions

The increase in absorbed solar radiation by the land surface in addition to the enhanced greenhouse effect at present implies thus even more stress on the terrestrial water cycle. The humidity paradox means that the Earth is warming and the atmosphere can hold more water vapour in an absolute sense, but the air over land is not as close to saturation as it once was. The latter is particularly relevant for regions where decreases in precipitation have occurred. The slower warming of the oceans at present means a limitation in evaporated moisture to keep pace with the rapid increase in the temperature over land. We assume that the humidity paradox doesn't exist during more gradual natural climate change since it goes slow enough in the ocean and over land so crossing of the vapour-liquid phase is not perturbed. The exception to a slow change in the climate, in an intimate historical time frame, is extreme cases of volcano eruptions, which are, however, relatively short-lived.

In summary, the higher warming rate over land than ocean, accelerating after 1980, is both the cause and the result of a positive feedback loop for terrestrial warming under rapid climate warming: An insufficient amount of water vapour proportional to atmospheric warming rates causes decreasing relative humidity over land, inhibiting cloud formation, increasing solar radiation, decreasing soil humidity, and hence accelerating terrestrial warming. As the ocean-land warming contrast and the

https://doi.org/10.5194/egusphere-2026-1654
Preprint. Discussion started: 2 April 2026

humidity paradox are direct consequences of rapid anthropogenic warming trends, decreasing cloud cover and increased solar radiation are likely a response to the CO2-driven warming. Overall, the topic requires more investigation. Opposite trends in precipitation between ERA5 and GPCP/GPCC appear over regions on Earth, particularly in Asia (Sect. 3.6). In addition, the present study did not investigate the initial cause of the proposed feedback loop, either if changes in humidity at the surface and in the air have been more important or reduced cloud cover. Based on 36 climate model simulations, Qu et al. (2014) found that the response of low clouds due to climate change is the largest source of uncertainty driving differences in climate sensitivity between the models.

https://doi.org/10.5194/egusphere-2026-1654
Preprint. Discussion started: 2 April 2026

Data and code availability

How to access ERA5 meteorological data from 1950 to the present is explained on the ECMWF website: https://confluence.ecmwf.int/display/CKB/How+to+download+ERA5#HowtodownloadERA5-OptionB:DownloadERA5familydatathatisNOTlistedintheCDSonlinecatalogue-SLOWACCESS. ERA5 data (Hersbach et al., 2023) were downloaded from the Copernicus Climate Change Service (C3S) Climate Data Store https://cds-beta.climate.copernicus.eu/datasets. The ERA5 data are generated using Copernicus Climate Change Service information (2023). Neither the European Commission nor ECMWF is responsible for any use that may be made of the Copernicus information or data it contains. The CERES radiation and skin temperature data were obtained from the NASA Langley Research Center, Atmospheric Science Data Center: https://ceres.larc.nasa.gov/data/. The CLARA-A3 radiation data can be find at EUMSAT CM SAF https://wui.cmsaf.eu/safira/action/viewDoiDetails?acronym=CLARA_AVHRR_V003. The HadISDH humidity data are found at https://www.metoffice.gov.uk/hadobs/hadisdh/. The Global Precipitation Climatology Project (GPCP) total precipitation data were downloaded from the Copernicus Climate Change Service: https://cds.climate.copernicus.eu/datasets/satellite-precipitation?tab=overview. Deutscher Wetterdienst GPCC Precipitation Analysis Climatology Version 2025 (at 0.5°): https://opendata.dwd.de/climate_environment/GPCC/html/gpcc_precipitation_analysis_climatology_v2025_doi_download.html. Temperature data from instrumental record over land and ocean for 1850 – 2020, presented in Figure 2.11c in Chapter 2.3.1.1.2 in IPCC, 2021, are found at https://data.ceda.ac.uk/badc/ar6_wg1/data/ch_02/ch2_fig11/v20220510. Information about Copernicus temperature indicators are found here: https://climate.copernicus.eu/climate-indicators/about-data.

The program MATLAB has been used to produce the results presented in the manuscript. The files are found here: https://stockholmuniversity.box.com/s/634bw9h0alv454p6rb3s4gyztm5nafj9

Author contributions

PG conceived and wrote the original draft. All authors together discussed the findings and contributed to the editing of the final manuscript produced for the review. PG produced all figures and tables.

Competing interests

The authors have no competing interests to declare.

https://doi.org/10.5194/egusphere-2026-1654
Preprint. Discussion started: 2 April 2026

Disclaimer

Publisher's note: Copernicus Publications remains neutral with regard to jurisdictional claims made in the text, published maps, institutional affiliations, or any other geographical representation in this paper. The authors bear the final responsibility for providing appropriate place names. Views expressed in the text are those of the authors and do not necessarily reflect the views of the publisher.

Acknowledgements

We acknowledge the Copernicus Climate Change Service for making the ERA5 reanalysis and GPCP data available. The CERES science project team is acknowledged for making the CERES satellite and ground-based data available. We acknowledge EUMETSAT CM SAF and Met Office Hadley Centre for making the CLARA-A3 radiation quantities and HadISDH humidity parameters, respectively, available. We acknowledge NOAA PSL, Boulder, Colorado, USA for Global Precipitation Climatology Project (GPCP) monthly analyses product data used in the present study. We acknowledge Deutscher Wetterdienst, Germany's National Meteorological Service, under the auspices of the World Meteorological Organisation (WMO) for Global Precipitation Climatology Centre (GPCC) monthly analyses data used in the present study.

Financial support

We acknowledge funding by the Swedish Research Council for Sustainable Development (FORMAS 2020-01000; 2023-01631) and from the Swedish Research Council, Vetenskapsrådet (grant number 2021-05143)."

Review statement

The review statement will be added by Copernicus Publications listing the handling editor as well as all contributing referees according to their status anonymous or identified.

https://doi.org/10.5194/egusphere-2026-1654
Preprint. Discussion started: 2 April 2026

References

Allan, R. A., Liu, C., Zahn, M., Lavers, D. A., Koukouvagias, E. and Bodas-Salcedo, A.: Physically Consistent Responses of the Global Atmospheric Hydrological Cycle in Models and Observations, Surv Geophys, 35, 533–552. DOI 10.1007/s10712-012-9213-z, 2014.

Allan, R. A., Barlow, M., Byrne, M. P., Cherchi, A., Douville, H., Fowler, H. J. et al.: Advances in understanding large-scale responses of the water cycle to climate change, Ann. N.Y. Acad. Sci., 1472, 49-75, 2020.

Allan, R. A., Willet, K. M., John, V. O. and Trent, T.: Global Changes in Water Vapor 1979 – 2020, Journal of Geophysical Research: Atmospheres, 127, 2022.

Artaxo, P., and Coauthors,: Tropical and Boreal Forest – Atmosphere Interactions: A Review, Tellus B: Chemical and Physical Meteorology, 74 (1), 24, https://doi.org/10.16993/tellusb.34, 2022.

Becker, A., Finger, P., Meyer-Christoffer, A., Rudolf, B. and Schamm, K.: A description of the global land-surface precipitation data products of the Global Precipitation Climatology Centre with sample applications including centennial (trend) analysis from 1901–present, Earth Syst. Sci. Data, 5, 71-99, https://doi.org/10.5194/essd-5-71-2013, 2023.

Berg, A., Findell, K., Lintner, B., Giannini, A., Seneviratne, S. I., van den Hurk, B. et al.: Land–atmosphere feedbacks amplify aridity increase over land under global warming, Nat. Clim. Chang., 6: 869–874, 2016.

Bojanowski, J. S. and Musial, J. P.: Dissecting effects of orbital drift of polar-orbiting satellites on accuracy and trends of climate data records of cloud fractional cover, Atmos. Meas. Tech., 13, 6771-6788, https://doi.org/10.5194/amt-13-6771-2020, 2020.

Bosilovich, M. G., Schubert, S. D. and Walker, G. K.: Global Changes of the Water Cycle Intensity, Journal of Climate, 18, 1591¬1608, 2005.

Boucher, O. et al.: Clouds and aerosols. In: Stocker TF, Qin D, Plattner GK, Tignor M, Allen SK, Boschung J, Nauels A, Xia Y, Bex V, Midgley PM (eds) Climate change 2013: the physical science basis. Contribution of Working Group I to the Fifth Assessment Report of the Intergovernmental Panel on Climate Change. Cambridge University Press, Cambridge, 2013.

Brogli, R., Sørland, S. L., Kröner, N. and Schär, C.: Future summer warming pattern under climate change is affected by lapse-rate changes. Weather Clim. Dynam., 2, 1093–1110. https://doi.org/10.5194/wcd-2-1093-2021, 2021.

Byrne, M. P. & O'Gorman, P. A.: Link between land-ocean warming contrast and surface relative humidities in simulations with coupled climate models, Geophys. Res. Lett., 40, 5223–5227, 2013.

Byrne, M. P. and O'Gorman, P. A., Understanding decreases in land relative humidity with global warming: conceptual model and GCM simulations, J. Climate, 29, 9045 – 9061, 2016.

https://doi.org/10.5194/egusphere-2026-1654
Preprint. Discussion started: 2 April 2026

Byrne, M. P. and O'Gorman, P. A.: Trends in continental temperature and humidity directly linked to ocean warming. P. Natl. Acad. Sci. USA, 115, 4863 – 4868, 2018.

Copernicus. Unprecedented Temperature Anomalies: On Track to Be The Warmest Year On Record (Copernicus Press Release), 2023.

Chandanpurkar, H. A., Famiglietti, J. S., Geopalan, K., Wiese, D. N., Wada, Y., Kakinuma, K. et al.: Unprecedented continental drying, shrinking freshwater availability, and increasing land contributions to sea level rise, Sci. Adv., 11, eadx0298, 2025.

Devasthale, A., Karlsson, K.-G. and Grassl, H.: Correcting orbital drift signal in the time series of AVHRR derived convective cloud fraction using rotated empirical orthogonal function, Atmos. Meas. Tech., 5, 267-273. doi:10.5194/amt-5-267-2012, 2012.

Devasthale, A. and Karlsson, K.-G.: Decadal Stability and Trends in the Global Cloud Amount and Cloud Top Temperature in the Satellite-Based Climate Data Records, Remote Sens., 15, 3819. https://doi.org/10.3390/rs15153819, 2023.

Devasthale, A., Andersson, S., Engström, E., Kaspar, F., Trentmann, J., Duguy-Tetzlaff, A. et al.: Leveraging the satellite-based climate data record CLARA-A3 to understand the climatic trend regimes relevant for solar energy applications over Europe, Earth. Syst. Dynam., 16, 1169-1182. https://doi.org/10.5194/esd-16-1169-2025, 2025.

Doelling, D. R. Loeb, N. G., Keyes, D. F., Nordeen, M. L., Morstad, D., Nguyen, C. et al.: Geostationary Enhanced Temporal Interpolation for CERES Flux Products, J. Atmos. Ocean. Technology, 30, 2023.

Doelling, D. R., Sun, M., Nguyen, L. T., Nordeen, M. L., Haney, C. O., Keyes, D. F. et al.: Advances in Geostationary-Derived Longwave Fluxes for the CERES Synoptic (SYN1deg) Product, J. Atmos. Ocean. Technology, 33, 2016.

Douville, H., Chauvin, F., Planton, S., Royer, J.-F., Salas-Mélia and Tyteca, S.: Sensitivity of the hydrological cycle to increasing amounts of greenhouse gases and aerosols, Climate Dynamics, 20, 45-68. DOI 10.1007/s00382-002-0259-3, 2002.

Douville, H. and Plazzotta, M.: Midlatitude summer drying: an underestimated threat in CMIP5 models?, Geophys. Res. Lett. 44: 9967–9975, 2017.

Douville, H., Qasmi, S., Ribes, A. and Back O.: Global warming at near-constant tropospheric relative humidity is supported by observations, Communications Earth & Environment, 3, 237, 2022.

Dufresne, J.-L. and Bony. S.: An assessment of the primary sources of spread of global warming estimates from coupled atmosphere–ocean models, J. Clim., 21, 5135–5144, 2008.

Dunn, R. J. H., Willett, K. M. and Ciavarella, A.: Comparison of land surface humidity between observations and CMIP5 models, Earth Syst. Dyn. 8: 719–747, 2017.

Gash, J. H. C. and Nobre, C. A.: Climatic Effects of Amazonian Deforestation: Some Results from ABRACOS, Bulletin of the American Meteorological Society. Vol. 78, No. 5, 1997.

Fang, Z., Zhang, W., Brandt, M., Abdi, A. M. and Fensholt, R.: Globally increasing atmospheric aridity over the 21st century, Earth's Future, 10, e2022EF003019. https://doi.org/10.1029/2022EF003019, 2022.

https://doi.org/10.5194/egusphere-2026-1654
Preprint. Discussion started: 2 April 2026

Flores, B. M., and Coauthors,: Critical transitions in the Amazon forest system, Nature,626 (7999), 555–564, https://doi.org/10.1038/s41586-023-06970-0, 2024.

Foster, G. and Rahmstorf, S.: Global warming has accelerated significantly, Geophysical Research Letters, 53, e2025GL118804. https://doi.org/10.1029/2025GL118804, 2026.

Gebrechorkos, S. H., Sheffield, J., Vicente-Serrano, S. M., Funk, C., Miralles, D. G., Peng, J. et al.: Warming accelerates global drought severity, Nature, Vol. 642, 628–635, https://doi.org/10.1038/s41586-025-09047-2, 2025.

Glantz, P., Fawole, O. G., Ström, J., Wild, M. and Noone, K. J.: Unmasking the effects of aerosols on greenhouse warming over Europe, J. Geophys. Res. Atmospheres, Vol. 127, Issue 22, https://doi.org/10.1029/2021JD035889, 2022.

Goessling, H. F., Rackow, T. and Jung, T.: Recent global temperature surge intensified by record-low planetary albedo, Science, Vol. 387, No 6729, DOI: 10.1126/science.adq7280, 2024.

Held, I. M. and Soden, B. J.: Water Vapour Feedback and Global Warming. Annu, Rev. Energy Environ., 25, 2000.

Held, I. M. and Soden, B. J.: Robust Responses of the Hydrological Cycle to Global Warming. Journal of Climate, 19, 5686 – 5699, 2006.

Hersbach, H., Peubey, C., Simmons, A. J., Berrisford, P., Poli, P. and Dee, D. P.: ERA-20CM: A twentieth-century atmospheric model ensemble, Quarterly Journal of the Royal Meteorological Society, 141 (691), 2350–2375, 2015.

Hersbach, H., Bell, B., Berrisford, P., Hirahara, S., Horányi, A., Muñoz-Sabater, J. et al.: The ERA5 global reanalysis, Quarterly Journal of the Royal Meteorological Society, 146, 1999 – 2049, 2020.

Hersbach, H., Bell, B., Berrisford, P., Biavati, G., Horányi, A., Muñoz Sabater, J. et al.: ERA5 monthly averaged data on single levels from 1940 to present. Copernicus Climate Change Service (C3S) Climate Data Store (CDS), DOI: 10.24381/cds.f17050d7, 2023.

Huffman, G., Adler, R. F., Behrangi, A., Bolvin D. T., Nelkin, E. J., et al.: The New Version 3.3 Global Precipitation Climatology Project (GPCP) Monthly and Daily Precipitation Products, Journal of Climate, 36, 7635-7655, DOI: 10.1175/JCLI-D-23-0123.1, 2023.

IPCC. Climate change 2001, Chapter 7.2.1: The physical science basis. In T. F. Stocker, et al. (Eds.), Contribution of Working Group I to the Third Assessment Report of the Intergovernmental Panel on Climate Change, Cambridge University Press, 2001.

IPCC. Climate change 2014: Synthesis report. In Contribution of Working Groups I, II and III to the Fifth Assessment Report of the Intergovernmental Panel on Climate Change, 2014.

IPCC. Climate change 2021, SPM A.1.2: The physical science basis. In V. Masson-Delmotte, et al. (Eds.), Contribution of Working Group I to the Sixth Assessment Report of the Intergovernmental Panel on Climate Change, Cambridge University Press, 2021.

Ishii, M., Fukuda, Y., Hirahara, S., Yasui, S., Suzuki, T. and Sato, K.: Accuracy of Global Upper Ocean Heat Content Estimation Expected from Present Observational Data Sets, SOLA, Vol. 13., 163−167, doi:10.2151/sola.2017-030, 2017.

https://doi.org/10.5194/egusphere-2026-1654
Preprint. Discussion started: 2 April 2026

Johannsen, F., Emida, S., Martins, J. P. A., Trigo, I. F., Nogueira, M. and Dutra, E.: Cold bias of ERA5 summertime daily maximum land surface temperature over Iberian Peninsula. Remote Sensing, 11 (21), 2570, 2019.

Karlsson, K.-G. et al.: CLARA-A2: the second edition of the CM SAF cloud and radiation data record from 34 years of global AVHRR data. Atm. Chem, Phys., 17, 5809–5828, www.atmos-chem-phys.net/17/5809/2017/, 2017.

Karlsson, K.-G., Stengel, M., Meirink, J. F., Riihelä, A., Trentmann, J., Akkermanns, T. et al.: CLARA-A3: The third edition of the AVHRR-based CM SAF climate data record on clouds, radiation and surface albedo covering the period 1979 to 2023, Earth Syst. Sci. Data, 15, 4901-4926, https://doi.org/10.5194/essd-15-4901-2023, 2023a.

Karlsson, K.-G., Stengel, M., Meirink, J. F., Riihelä, A., Trentmann, J., Akkermanns, T. et al.: CLARA-A3: CM SAF cLoud, Albedo and surface RAdiation dataset from AVHRR data – Edition 3, Satellite Application Facility on Climate Monitoring [data set], https://doi.org/10.5676/EUM_SAF_CM/CLARA_AVHRR/V003, 2023b.

Kato, S., Rose, F. G., Doelling, D. R., Rutan, D.a., Caldwell, T. E., Yu, L. and Weller, R. A.: Surface irradiances consistent with CERES-derived top-of-atmosphere shortwave and longwave irradiances, J. Climate, 26, 2719–2740. https://doi.org/10.1175/JCLI-D-12-00436.1, 2013.

Kato, S., Rose, F. G., Rutan, D. A., Thorsen, T. J., Loeb, N. G., Doelling, vid R. et al.: Surface Irradiances of Edition 4.0 Clouds and the Earth's Radiant Energy System (CERES) Energy Balanced and Filled (EBAF) Data Product, Journal of Climate, 31, 2018.

Kendall, M. G. Rank: Correlation Methods, 4th edition, Charles Griffin, London, 1975.

Kosaka, Y., S. Kobayashi, Y. Harada, C. Kobayashi, H. Naoe, K. et al.: The JRA-3Q reanalysis, J. Meteor. Soc. Japan, 102, 49-109, https://doi.org/10.2151/jmsj.2024-004., 2024.

Li, H., Insua-Costa, D., Koppa, A., Geirinhas, J. L., Keune, J. et al.: Observational evidence of compensatory influences of deforestation on downwind precipitation in Brazilian breadbaskets, npj Clim. Atmos. Sci., 8:279, https://doi.org/10.1038/s41612-025-01152-3, 2025.

Li, Y., Li, Z.-L., Wu, H. et al.: Biophysical impacts of earth greening can substantially mitigate regional land surface temperature warming. Nature Communication, 14:121, https://doi.org/10.1038/s41467-023-35799-4, 2023.

Liu, H., Koren, I., Altaratz, O. and Chekroun, M. D.: Opposing trends of cloud coverage over land and ocean under global warming, Atmos. Chem. Phys., 23, 6559-6569, https://doi.org/10.5194/acp-23-6559-2023, 2023.

Loeb, N. G., Doelling, D. R., Wang, H., Nguyen, C., Corbett, J. G., Liang, L. et al.: Clouds and the Earth's Radiant Energy System (CERES) Energy Balanced and Filled (EBAF) Top-of-Atmosphere (TOA) Edition-4.0 Data Product, Journal of Climate, 31, 2018.

Loeb, N. G., Johnson, G. C., Thorsen, T. J., Lyman, J. M., Rose, F. G., Kato S. et al.: Satellite and Ocean Data Reveal Marked Increase in Earth's Heating Rate, Geophysical Research Letters, 48, https://doi.org/10.1029/2021G L093047, 2021.

Loeb, N. G., Ham, S.-H., Allan, R. P., Thorsen, T. J., Meyssignac, B., Kato, S. et al.: Observational Assessment of Changes in Earth's Energy Imbalance Since 2000, Surveys in Geophysics, 45(6), 1757-1783, doi:10.1007/s10712-024-09838-8, 2024.

https://doi.org/10.5194/egusphere-2026-1654
Preprint. Discussion started: 2 April 2026

Luo, H., Quaas, J. and Han, Y.: Diurnally asymmetric cloud cover trends amplify greenhouse warming, Science Advances, 10, eado5179, 2024a.

Luo, H., Quaas, J. and Han. Y.: Decreased cloud cover partially offsets the cooling effects of surface albedo change due to deforestation, Nature Communication, https://doi.org/10.1038/s41467-024-51783-y, 2024b.

Manabe, S., Stouffer, R. J., Spelman, M. J. and Bryan, K.: Transient responses of a coupled ocean-atmosphere model to gradual changes of atmospheric CO2. Part 1: Annual mean response, J. Clim., 4, 785– 818, 1991.

Manabe, S.: Role of greenhouse gas in climate change, Tellus A., 71, 1620078, https://doi.org/10.1080/16000870.2019.1620078, 2019.

Martens, B., Schumacher, D. L., Wouters, H., Muñoz-Sabater, J, Verhoest, N. E. C. and Miralles, D. G.: Evaluating the land-surface energy partitioning in ERA5, Geosci, Model Dev., 13, 4159–4181, https://doi.org/10.5194/gmd-13-4159-2020, 2020.

Mudryk, L., Santolaria-Otín, M., Krinner, G., Ménégoz, M., Derksen, C., Brutel-Vuilmet, C., Brady, M.and Essery, R.: Historical Northern Hemisphere snow cover trends and projected changes in the CMIP6 multi-model ensemble. The Cryosphere, 14, 2495–2514. https://doi.org/10.5194/tc-14-2495-2020, 2020.

Mudryk, L., Chereque, E., Brown, R., Derksen, C., Luojus, K. and Decharme, B.: The Arctic: Terrestrial snow cover [in "State of the Climate in 2021"], Bull. Amer. Meteor. Soc**., 102** (8), S287–S290, https://doi.org/10.1175/BAMS-D-21-0086.1, 2021.

Myers-Smith, I. H., Kerby, J. T., Phoenix, G. K., Bjerke, J. W., Epstein, H. E., Assmann, J. J. et al.: Complexity revealed in the greening of the Arctic, Nat. Clim. Chang., 10, 106–117, https://doi.org/10.1038/s41558-019-0688-1, 2020.

Næss, F. W., Devasthale, A., Ekman, A. M. L. and Hannashi, A.: A climatological perspective on trends and variability of cloudiness over the Amazonian basin during the last decades, Journal of Climate, DOI 10.1175/JCLI-D-24-0747.1, 2025.

Quintanilla, M., and Coauthors: Investigative research conducted by the Red Amaz´onica de Informaci´on Socioambiental Georreferenciada (RAISG) within the framework of the Initiative "Amazonia for Life: protect 80% by 2025" and coordinating organizations COICA and Stand.earth, 2025.

Phoenix, G. K., Bjerke, J. W., Björk, R. G. , Blok, D., Bryn, A., Callaghan, T. V. et al.: Browning events in Arctic ecosystems: Diverse causes with common consequences, PLOS Clim 4(1): e0000570, https://doi.org/10.1371/journal.pclm.0000570, 2025.

Qu, X., Hall, A., Klein, S. A. and Caldwell. P. M.: On the spread of changes in marine low cloud cover in climate model simulations of the 21st century, Clim. Dyn., 42:2603–2626, DOI 10.1007/s00382-013-1945-z, 2014.

Quaas, J., Jia, H., Smith, C., Albright, A. L., Aas, W., Bellouin, N. et al.: Robust evidence for reversal of the trend in aerosol effective climate forcing, Atmos. Chem. and Phys., 22, 12221 – 12239, 2022.

Rantanen, M. and Laaksonen, A.: The jump in global temperatures in September 2023 is extremely unlikely due to internal climate variability alone, Climate and Atmospheric Science, 7:34, 2024.

Rose, F. G., Rutan, D. A., Charlock, T., Smith, G. L. and Kato, S.: An algorithm for the constraining of radiative transfer calculations to CERES-observed broadband top-pf-atmosphere irradiance. J. Atmos. Oceanic Technol, 30, 1091-1106. 1091–1106 https://doi.org/10.1175/JTECH-D-12-00058.1, 2013.

Schmidt, G.: Why 2023's heat anomaly is worrying scientists, Nature, 67, 467, 2024.

https://doi.org/10.5194/egusphere-2026-1654
Preprint. Discussion started: 2 April 2026

Schneider, T., O'Gorman, P. A. and Levine, X. J.: Water vapor and the dynamics of climate change, Rev. Geophys., 48, RG3001, doi:10.1029/2009RG000302, 2010.

Schneider, T., Kaul, C. M. and Pressel, K. G.: Possible climate transitions from breakup of stratocumulus decks under greenhouse warming, Nature Geoscience, 12, 163–167, 2010.

Schneider, T., Teixeira, J., Bretherton, C. S., Brient, F., Pressel, K. G., Schär, C. and Siebesma, A. P.: Climate goals and computing the future of clouds, Nat. Clim. Chang., 7, 2017.

Schneider, U., Becker, A., Finger, P., Meyer-Christoffer, A., Ziese and Rudolf, B.: GPCC's new land surface precipitation climatology based on quality-controlled in situ data and its role in quantifying the global water cycle, Theor. Appl. Climatol., 115, 15-40, DOI 10.1007/s00704-013-0860-x, 2014.

Schulz, J., Albert, P., Behr, H.-D., Caprion, D., Deneke, H., Dewitte, S. et al. (2009), Operational climate monitoring from space: the EUMETSAT Satellite Application Facility on Climate Monitoring (CM-SAF). Atmos. Chem. Phys., 9, 1687-1709. www.atmos-chem-phys.net/9/1687/2009/

Sherwood, S. C., Webb, M. J., Annan, J. D., Armour, K. C., Forster, P. M., Hargreaves, J. C., et al.: An assessment of Earth's climate sensitivity using multiple lines of evidence, Reviews of Geophysics, 58, e2019RG000678, https://doi.org/10.1029/2019RG000678, 2020.

Simmons, A. J., Willett, K. M., Jones, P. D., Thorne, P. W. and Dee, D. P.: Low-frequency variations in surface atmospheric humidity, temperature, and precipitation: Inferences from reanalyses and monthly gridded observational data sets. J. Geophys. Res., 115, 2010.

Simmons, A. J.: Trends in the tropospheric general circulation from 1979 to 2022, Weather Clim. Dynam., 3, 777-809, https://doi.org/10.5194/wcd-3-777-2022, 2022.

Smith, S. J., van Aardenne, J., Klimont, Z., Andres, R. J., Volke, A., and Delgado Arias, S.: Anthropogenic sulfur dioxide emissions: 1850–2005, Atmospheric Chemistry and Physics, 11(3), 1101–1116, https://doi.org/10.5194/acp-11-1101-2011, 2011b.

Smith, A., Lott, N. and Vose, R.: The Integrated Surface Database: Recent Developments and Partnerships, Bulletin of the American Meteorological Society, 92, 704-708, doi:10.1175/2011BAMS3015.1, 2011a.

Soden, B. J. and Held, I. M.: An assessment of climate feedbacks in coupled ocean atmosphere models, J. Clim. 19, 3354–3360, 2006.

Sutton, R. T., Dong, B. and Gregory, J. M.: Land/sea warming ratio in response to climate change: IPCC AR4 model results and comparison with observations. Geophys. Res. Let., 34, L02701. doi:10.1029/2006GL028164, 2007.

Tegen, I., Hollrig, P., Chin, M., Fung, I., Jacob, D., and Penner, J.: Contribution of different aerosol species to the global aerosol extinction optical thickness: Estimates from model results, J. Geophys. Res., 102 (D20), 23895–23915, 1997.

Trenberth, K. E., Smith L., Quin, T., Dai, A. and Fasullo, J.: Estimates of the Global Water Budget and Its Annual Cycle Using Observational and Model Data, Journal of Hydrometeorology, Vol. 8, Issue 4, 758–769, https://doi.org/10.1175/JHM600.1, 2007.

https://doi.org/10.5194/egusphere-2026-1654
Preprint. Discussion started: 2 April 2026

Trenberth, K. E., and Cheng, L.: Earth's Energy Balance, Reference Module in Earth Systems and Environmental Sciences, Elsevier, 2024, ISBN 9780124095489, https://doi.org/10.1016/B978-0-323-96026-7.00039-4, 2024.

Tselioudis, G., Remillard, J., Jakob, C. and Rossow, W. B.: Contraction of the World's Storm-Cloud Zones the Primary Contributor to the 21st Century Increase in the Earth's Sunlight Absorption, Geophys. Res. Lett., 52, e2025GL114882, https://doi.org/10.1029/2025GL114882, 2025.

Vial, J., Dufresne, J.-L. and Bony, S.: On the interpretation of inter-model spread in CMIP5 climate sensitivity estimates, Clim. Dyn., 41, 3339–3362, 2013.

Wan, N., Lin., X., Pielke Sr, R. A., Zeng, X. and Nelson, A. M.: Global total precipitable water variations and trends over the period 1958–2021, Hydsol. Earth Syst. Sci, 28, 2123-2137, https://doi.org/10.5194/hess-28-2123-2024, 2024.

Wang, J., Pan, F., An, P., Han, G., Jiang, K., Song, Y. et al.: Atmospheric Water Vapor Transport between Ocean and Land under Climate Warming, Journal of Climate, Vol. 36, Issue 17, 5861–5880, https://doi.org/10.1175/JCLI-D-22-0106.1, 2023.

Wilcoxon, F.: Individual Comparisons by Ranking Methods. Biometrics Bulletin, 1, No. 6, 80-83, https://www.jstor.org/stable/3001968, 1945.

Willet, K. M. Dunn, R. J. H., Thorne, P. W., Bell, S., de Podesta, M., Parker, D. E. et al.: HadISDH land surface multi-variable humidity and temperature record for climate monitoring, Clim. Past., 10, 1983-2006, 2014.

Willet, K. M., Simmons, A. J., Bosilovich, M, and Lawers, D. A.: Hydrological cycle ¬ atmosphere [in "State of the Climate in 2023"], Bull. Amer. Meteor. Soc., 105 (8), S52–S52, https://doi.org/10.1175/BAMS-D-24-0116.1, 2024.

Wong, E. W. and Minnett, P. J.: The Response of the Ocean Thermal Skin Layer to Variations in Incident Infrared Radiation, J. Atmos. Res.: Oceans, 123, 2475-2493, https://doi.org/10.1002/2017JC013351, 2018.

Woolings, T., Drouard, M., O'Reilly, C. H., Sexton, D. M., and McSweeney, C.: Trends in the atmospheric jet streams are emerging in observations and could be linked to tropical warming, Communications Earth & Environment, 4, 125, https://doi.org/10.1038/s43247-023-00792-8, 2023.

World Meteorology Organization (WMO): Temperatures in Europe increase more than twice global average. https://public.wmo.int/en/media/press-release/temperatures-europe-increase-more-twice-global-average, 2022.

Zelinka, M. D., Randall, D. A., Webb, M. J. and Klein, S. A.: Clearing clouds of uncertainty, Nat. Clim. Chang., 7, 674–678, 2017.

Zhuang et al.: Anthropogenic warming has ushered in an era of temperature-dominated droughts in the western United States, Science Advances, 10. 1-13, 2024.